Chinese Journal of Chemical Engineering 42 (2022) 297–311

Contents lists available at ScienceDirect

Chinese Journal of Chemical Engineering

journal homepage: www.elsevier.com/locate/CJChE

Review

Two-dimensional graphitic carbon nitride for membrane separation

Tao Zheng [1,2], Xiuyang Zou [1], Meisheng Li [1,*], Shouyong Zhou [1], Yijiang Zhao [1,2,*], Zhaoxiang Zhong [2]

[1] *Jiangsu Engineering Laboratory for Environment Functional Materials, Jiangsu Key Lab for Chemistry of Low-Dimensional Materials, School of Chemistry and Chemical Engineering, Huaiyin Normal University, Huaian 223300, China*

[2] *State Key Laboratory of Materials-Oriented Chemical Engineering, National Engineering Research Center for Special Separation Membrane, Nanjing Tech University, Nanjing 210009, China*

ARTICLE INFO

Article history:
Received 3 September 2020
Received in revised form 24 January 2021
Accepted 24 January 2021
Available online 10 March 2021

Keywords:
Two-dimensional (ZD)
g-C_3N_4
Membranes
Separation

ABSTRACT

Recent years, membrane separation technology has attracted significant research attention because of the efficient and environmentally friendly operation. The selection of suitable materials to improve the membrane selectivity, permeability and other properties has become a topic of vital research relevance. Two-dimensional (2D) materials, a novel family of multifunctional materials, are widely used in membrane separation due to their unique structure and properties. In this respect, as a novel 2D material, graphitic carbon nitride (g-C_3N_4) have found specific attention in membrane separation. This study reviews the application of carbon nitride in gas separation membranes, pervaporation membranes, nanofiltration membranes, reverse osmosis membranes, ion exchange membranes and catalytic membranes, along with describing the separation mechanisms.

1. Introduction

Membrane separation technology emerged at the beginning of the 20th century, and it is a vital technology for separation, concentration and purification of materials [1]. This technology has the characteristics of high efficiency, energy saving, environmental friendliness, molecular level filtration and easy to control filtration process [2]. Therefore, the membrane separation technology has been widely employed in diverse fields, such as food, medicine, biology, environmental protection, chemical industry, metallurgy, energy, petroleum, water treatment, electronics, bionics *etc*. [3–5]. Overall, it has become one of the most important means of separation, along with leading to significant economic and social benefits [1,2]. Traditional three-dimensional (3D) membranes prepared from 3D materials have stable structure and outstanding performance. However, Compared to 2D membrane, 3D membrane is difficult to prepare and its structure is complex and difficult to control. At the some time, the membrane-forming performance of 2D materials is better than that of 3D materials [6,7]. In fact, an increasing number of new materials have been used in the preparation of membranes to achieve additional functionalities (photoelectric conversion, catalysis, *etc*.) [8,9]. For instance, Tsapatsis *et al*. (2011) prepared a new separation membrane (ZSM-5) with zeolite nanosheets [10]. Since then, the development of high-performance separation membranes from 2D materials has become a topic of significant research interest. In contrast with 3D membranes, 2D membranes can be one-atom to a few atoms thick, therefore, these exhibit less resistance and high flux. Particularly, a high extent of separation is possible by adjusting the pore size of 2D nanosheets and interlayer channels of adjacent nanosheets [10–12]. Thus these advantages have made 2D nanosheets membranes the superb candidates for high-performance separation. Graphene and its derivatives are one of the most widely studied 2D materials. Since 2012, graphene-based separation membranes have received widespread attention [13,14]. Apart from graphene and its derivatives, other emerging 2D nanosheet materials including 2D zeolites, 2D metal–organic frameworks (MOFs), 2D covalent-organic frameworks (COFs), MXenes and graphitic carbon nitrides (g-C_3N_4) have also exhibited an unprecedented potential in microfiltration, nanofiltration, ultrafiltration, reverse osmosis, pervaporation and gas separation [15–17]. g-C_3N_4, a novel non-metallic photocatalytic material, is mainly used in the field of catalysis because of its superior catalytic properties as compared to the existing materials [18,19]. g-C_3N_4 has unique photoelectric properties and is easily stimulated by light to produce electron-hole pairs. g-C_3N_4 is a planar 2D lamellar structure similar to graphene and the flexibility of g-C_3N_4 is better

* Corresponding authors.
E-mail addresses: lms1108@hytc.edu.cn (M. Li), cyjzhao@126.com (Y. Zhao).

https://doi.org/10.1016/j.cjche.2021.01.011
1004-9541/

than 3D materials. g-C_3N_4 nanosheets with single atomic layers can be prepared. In recent years, the potential of g-C_3N_4 in the field of membrane separation has been continuously explored due to its unique structure and excellent performance [20,21]. Form Fig. 1, it can be seen that the g-C_3N_4 has been applied in gas separation membranes, pervaporation membranes, nanofiltration membranes, reverse osmosis membranes, ion exchange membranes, catalytic membranes, and so on.

This review is structured as follows: Section 2 reviews the structure and methods to prepare g-C_3N_4, whereas; Section 3 discusses the industrial applications of g-C_3N_4 in gas separation membranes, pervaporation membranes, nanofiltration membranes, reverse osmosis membranes, ion exchange membranes and catalytic membranes. The role of g-C_3N_4 in these membranes has been correlated with the structure and properties of the membranes. Finally, the conclusions and some guidelines for future work are presented in Section 4.

2. Structure and Preparation of g-C_3N_4

Carbon nitride (C_3N_4) is known to be one of the oldest synthetic compounds. In 1996, Teter *et al.* employed the first-principles calculations and proposed that the C_3N_4 has 5 structures including g-C_3N_4 [28]. g-C_3N_4 exhibits a 2D planar lamellar structure similar to graphene, with triazine (C_3N_3) and 3-s-triazine (C_6N_7) rings as the basic structural units, extending indefinitely to form a network structure [29,30]. Kroke *et al.* reported that the structure of 3-s-triazine ring is more stable than the triazine ring and the 2D nanosheet layers are held together by van der Waals forces with using density functional theory (DFT) [31]. Due to the presence of 3-s-triazine ring structure, the g-C_3N_4 layer is observed to have many pores [29–31]. Fig. 2 shows that the distance between the two adjacent atomic layers of g-C_3N_4 is observed to be 0.326 nm, whereas the molecular kinetic diameter of the pore is 0.311 nm [28–30].

There are four main preparation methods for g-C_3N_4, including solid phase reaction, solvent-thermal, electrochemical deposition and thermal polymerization [32–36]. Synthesis of g-C_3N_4 by solid-phase reaction generally selects compounds containing triazine structure as reaction precursors, such as melamine and melamine, and uses LiN_3 and NaN_3 as nitrogen sources. g-C_3N_4 should be prepared by solid phase reaction at a certain temperature. The method can flexibly adjust the C/N molar ratio and the nanostructure and morphology of the controllable material. Generally, g-C_3N_4 is prepared by solvent thermal method with melamine, melamine and chlorine as raw materials, and NH_2NH_2 and Et_3N as solvent under a certain temperature. The method has the advantages of mild reaction conditions, easy control and good uniformity of the system. In recent years, electrochemical deposition has been applied to the preparation of g-C_3N_4 thin films. This method is simple, easy to control and can reduce the temperature of the reaction system. Thermal polymerization is a direct and simple material preparation method, which forms g-C_3N_4 through the condensation polymerization of precursors induced by heat. The thermal polymerization method has evolved as the preferred way to prepare g-C_3N_4 on a large scale due to its several advantages, including ability to employ different precursors, low cost, moderate equip-

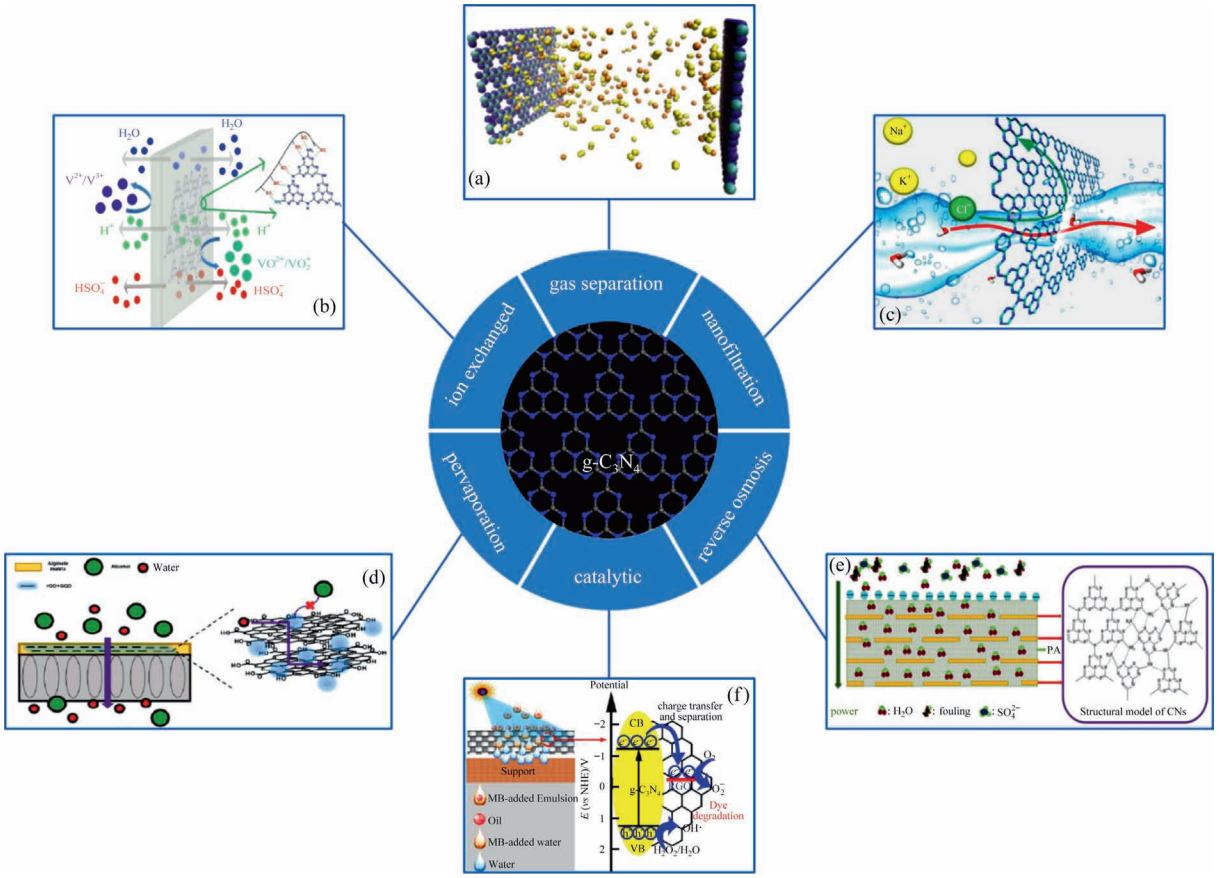

Fig. 1. (a) The schematic diagram of mixed gas permeation setup [22]; (b) The proposed mechanism for proton transport in vanadium ion permeation process in hybrid membrane [23]; (c) The schematic of water-salt separation process by nanoporous g-C_3N_4 membranes [24]; (d) The schematic illustration of the preparation of graphene oxide and polyelectrolyte complex nanohybrid membranes [25]; (e) The schematic of water-salt separation process and antifouling process of PA/CNs membrane [26]; (f) The schematic illustration of oil/water separation and photocatalytic degradation process in the composite membrane [27].

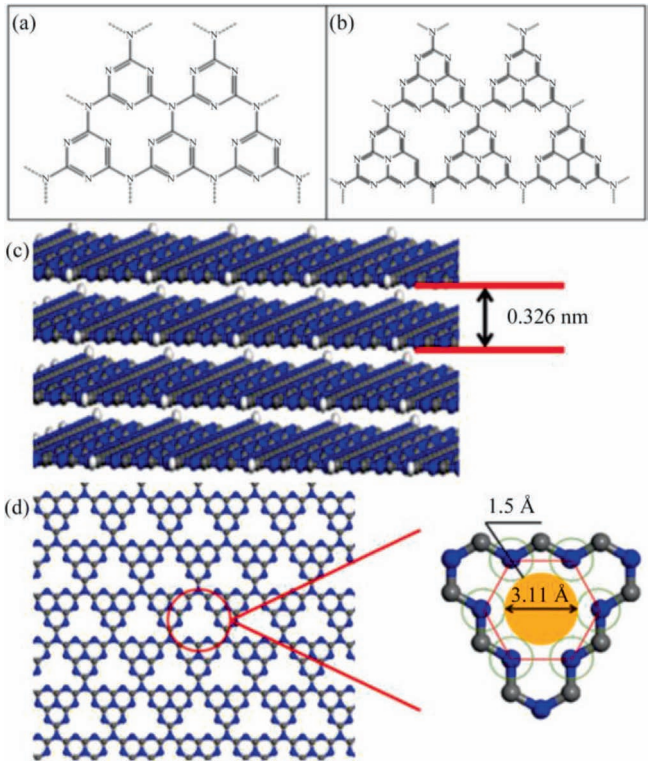

Fig. 2. Molecular structure diagram of g-C_3N_4 [28–30]: (a) C_3N_3 and (b) C_6N_7; The schematic diagram of g-C_3N_4 molecular model: (c) Layers and (d) Pores. (1Å = 0.1 nm)

ment and control requirement, simple operation and easy amplification. Initially, g-C_3N_4 was applied in the field of catalysis [37,38]. Compared to conventional metal oxide catalysts (Fe_2O_3, TiO_2, ZnO, *etc.*) [39–42], g-C_3N_4 has a wider spectrum of absorption [43,44]. Especially, g-C_3N_4 can perform photocatalysis in normal visible light without the need for ultraviolet light. As a classical 2D material, g-C_3N_4 has unique structural characteristics different from traditional 3D materials. g-C_3N_4 has good thermal stability, chemical stability, acid and alkaline resistance, and it is non-toxic and environmentally friendly. In recent years, g-C_3N_4 has gained widespread research attention due to its unique structure and excellent performance. Therefore, the potential of g-C_3N_4 in the field of energy is constantly being explored [45,46].

3. Application of g-C_3N_4 in Membranes

3.1. Gas separation membranes

A gas separation membrane is mainly used to screen gas molecules of different sizes through pores or holes [47–49]. The same function can be achieved through the holes developed in materials [48,49]. Therefore, g-C_3N_4 has been used to separate gases using the pores on the surface. The gas separation mechanism for the g-C_3N_4 membrane is proposed in Fig. 3. Also, g-C_3N_4 can be used to modify the original pores of the membranes to prepare mixed matrix membranes (MMMs) to improve the separation performance [50,51]. Alternatively, the pores can also absorb gas molecules, and the adsorption effect is different for different molecules, thus, leading to their separation due to this characteristic [52,53]. At present, most of the research focuses on H_2 separation and purification. Due to the structure, only molecules (H_2, H_2O, *etc.*) smaller than the pore size of g-C_3N_4 can pass freely

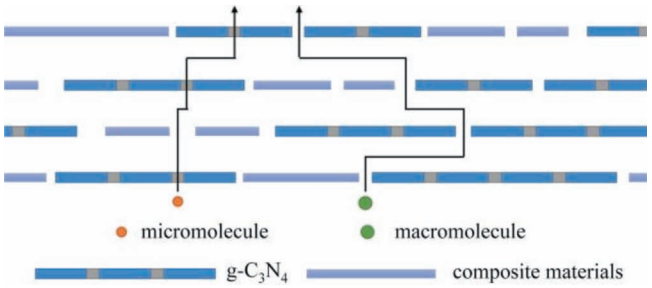

Fig. 3. Schematic diagram of gas separation membranes prepared by g-C_3N_4.

through the g-C_3N_4 sheets. So, the separation and purification of H_2 by g-C_3N_4 is feasible and easy to be realized.

In 2015, Li *et al.* [22] demonstrated using first-principles calculations that as-synthesized g-C_3N_4 exhibited high efficiency of helium separation from the gas molecules (H_2, N_2, CO and CH_4) in natural gas and the noble gas molecules (Ne and Ar). For the transition state calculations, the authors performed the minimum energy path profiling using the climbing image nudged elastic band method (CNEB) implemented in the VASP transition state tools. The most energetically favorable configuration of a gas molecule on the g-C_3N_4 membrane was determined through structural optimization. The authors observed that the gas molecules prefer to reside right above the pores at different heights depending on the specific gas. Through the energy barrier analysis, the diffusion rates and selectivities of different molecules for g-C_3N_4 at different temperature were studied. In addition, the authors analyzed the steered molecular dynamics (MD) simulation for separating He from H_2 and ^{3}He from ^{4}He. The energy barrier for the He molecule passing through the g-C_3N_4 membrane was calculated to be 0.354 eV, however, the selectivity over H_2 at room temperature was predicted to be as high as 10^7. More interestingly, g-C_3N_4 served as an efficient quantum sieving membrane for ^{3}He/^{4}He separation with a predicted transmission ratio of 18 at 49 K. The observed results offer a promising membrane system for separating ^{3}He from natural gas, which is quite crucial for cryogenic industries. It was for the first time that g-C_3N_4 could be applied to gas separation membranes by using the theoretical calculations. In the following years, further research efforts proved the feasibility of such process. By using the first-principles calculations and molecular dynamics simulations, Ji *et al.* concluded that the porous g-C_3N_4 monolayer works as an efficient and highly selective hydrogen purification membrane [54]. The results indicated that the g-C_3N_4 nanosheets exhibit a significant potential for separating H_2 from undesirable gases. Using a combination of density functional theory (DFT) and MD simulations, de Silva *et al.* demonstrated that g-C_3N_4 can effectively purify H_2 from CO_2 and CH_4 [55]. The theoretical analysis employed by the authors indicated that the flux can be significantly improved by widening the pore area by applying biaxial strains as low as 2.5% and 5%. It was also observed that the strain tuning only improves the H_2 permeability of the membrane, while its excellent H_2/CO_2 and H_2/CH_4 selectivity is not compromised. In 2019, Guo *et al.* studied the separation of H_2 from the impurity gases (H_2, N_2, H_2O, CO, Cl_2, and CH_4) by using the bilayer porous g-C_3N_4 membrane with DFT [56]. The studies highlighted a new approach towards achieving high permeance and high selectivity molecular-sieving membranes for simple structural engineering.

From Fig. 4, it can be noted that the separation and purification of hydrogen from common components can be effectively achieved with g-C_3N_4. Thus, it is theoretically proved that g-C_3N_4 can be used to prepare gas separation membranes. In addition to the theoretical calculations, the researchers have carried out experimental

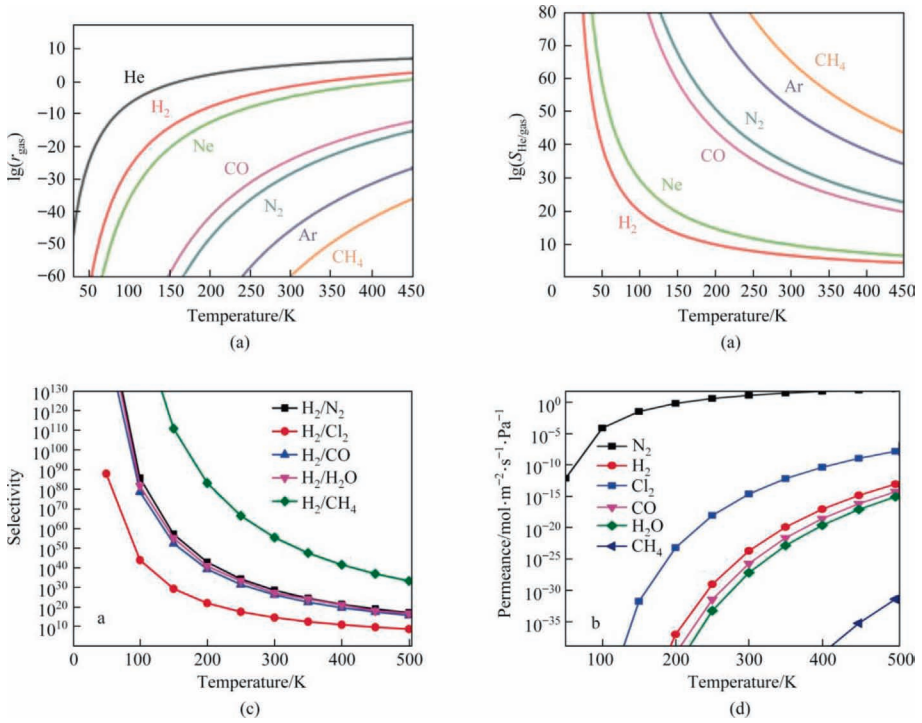

Fig. 4. The transmission rate (a) and selectivity (b) of gas molecules passing through the pores on the g-C_3N_4 membrane as a function of temperature [22]; The plots of (c) selectivity and (d) permeance versus temperature for H_2, O_2, N_2, Cl_2, CO, CH_4 and H_2O molecules passing through the bilayer g-C_3N_4 [56].

efforts to explore the use of g-C_3N_4 in gas separation in recent years. In 2016, Tian *et al.* prepared novel mixed matrix membranes (MMMs) by incorporating the g-C_3N_4 nanosheets into the polymer matrices exhibiting intrinsic microporosity (PIM-1, Fig. 5) [49]. The pure gas permeation tests of the MMMs were conducted for CO_2, CH_4, N_2 and H_2.

The results showed that g-C_3N_4 displayed a pronounced effect, on the gas transport within PIM-1/g-C_3N_4 MMMs. Firstly, the 2D structured g-C_3N_4 effectively influenced the packing of the polymer chains owing to the high aspect ratio. Correspondingly, the gas permeability of MMMs was significantly enhanced at a relatively low g-C_3N_4 mass loading of 1%, as compared with the pure PIM-1 membrane. Moreover, the periodic ultramicropores of g-C_3N_4 with size-sieving effect preferentially facilitated the transport of smaller molecules (especially, H_2), and the selectivities for H_2/CH_4 and H_2/N_2 were observed to increase without compromising the gas permeability, as compared with pure PIM-1. The thermal and mechanical properties of the MMMs were also noted to improve with the incorporation of g-C_3N_4. Furthermore, the PIM-1/g-C_3N_4 MMMs demonstrated superior long-term performance even at low g-C_3N_4 loading (see Tables 1 and 2).

Hou *et al.* [57] proposed rapid in-situ fabrication of zeolitic imidazolate framework-8 (ZIF-8) hybrid membrane by using the 2D g-C_3N_4 nanosheets at room temperature. The chemical structure of g-C_3N_4 and the preparation process are shown in Fig. 6. The negatively charged g-C_3N_4 nanosheets with abundant nitrogen coordinating sites are capable of capturing and anchoring Zn^{2+}, thus,

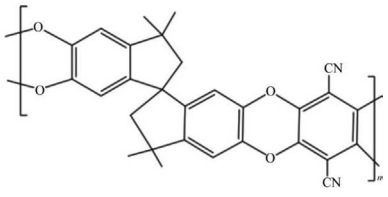

Fig. 5. Chemical structure of PIM-1 [49].

Table 1
Mechanical properties of pure PIM-1 and PIM-1/g-C_3N_4 MMMs [49].

Membrane	Tensile strength/ MPa	Elongation at break/%	Young's modulus/ GPa
PIM-1	40.93	4.03	2.13
PIM-1-g-C_3N_4(0.5)	46.94	4.40	2.79
PIM-1-g-C_3N_4(1.0)	52.90	6.43	2.85
PIM-1-g-C_3N_4(1.5)	49.65	6.20	2.74
PIM-1-g-C_3N_4(2.0)	44.81	4.75	2.31

Table 2
Selectivity of as-cast pure PIM-1 and PIM-1/g-C_3N_4 MMMs for various gas pairs [49]

Membrane	CO_2/N_2	CO_2/CH_4	H_2/N_2	H_2/CH_4
PIM-1	23.1	15.0	13.1	8.5
PIM-1-g-C_3N_4(0.5)	19.9	12.4	14.4	9.0
PIM-1-g-C_3N_4(1.0)	16.3	11.5	10.8	7.6
PIM-1-g-C_3N_4(1.5)	15.6	11.7	13.2	9.9
PIM-1-g-C_3N_4(2.0)	19.8	14.4	16.4	11.9

providing a large number of heterogeneous nucleation sites for the formation of initial ZIF-8 crystals. During the cyclical spin coating of the Zn^{2+}/g-C_3N_4 nanosheets and ligand (2-methylimidazole), the in-situ formed ZIF-8 crystal nuclei on the g-C_3N_4 nanosheets promote the further growth of the continuous defect-free membranes. The ZIF-8/g-C_3N_4 membranes with a thickness of 240 nm can be obtained using this methodology within 30 min at room temperature, which represents an attractive attribute for fast and facile preparation of the molecular sieving membranes. Moreover, a promising H_2/CO_2 separation performance with the selectivity up to 42 are observed, which is superior to the other ZIF-8 membranes.

For the separation of CO_2/CH_4 system, Maria *et al.* [58] protonized, hydroxylated and hydrated g-C_3N_4. As shown in Fig. 7, The authors subsequently doped Matrimid with protonated g-

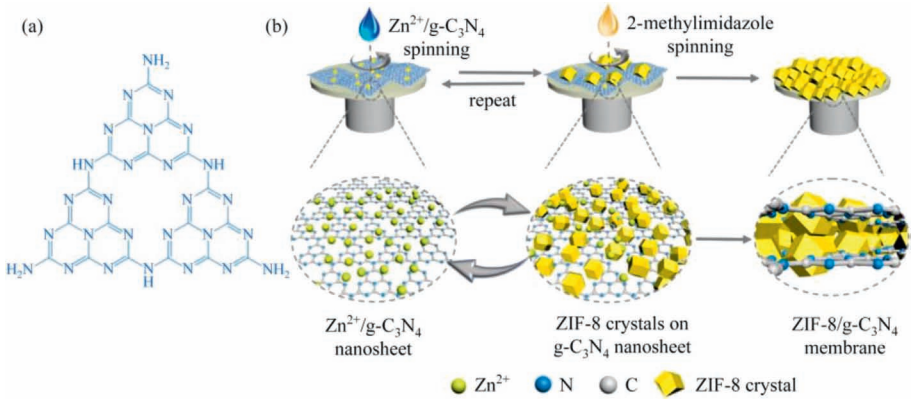

Fig. 6. (a) The chemical structure of g-C_3N_4; (b) The schematic illustration of the preparation of the molecular sieving membrane with assistance of the g-C_3N_4 nanosheets *via* cycled spin coating [57].

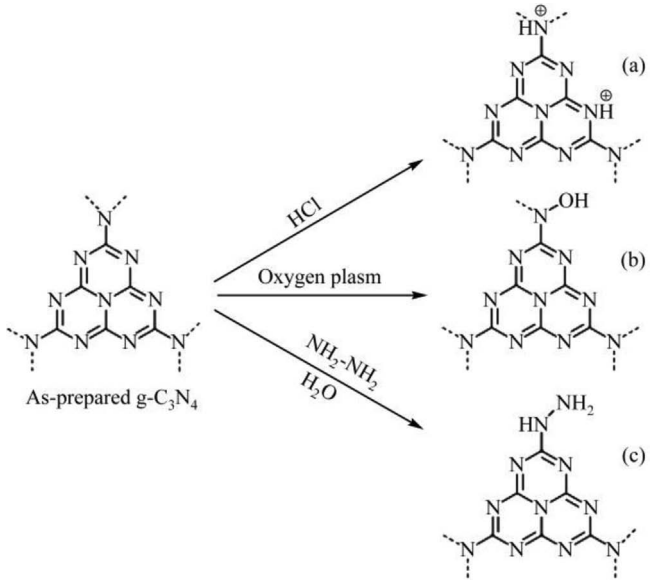

Fig. 7. The schematic of the synthesis of: (a) protonated g-C_3N_4; (b) oxygen plasm treatment used to introduce hydroxylamine structure (N-OH) on the surface of g-C_3N_4 (hydroxylaminated g-C_3N_4); and (c) hydrazinated g-C_3N_4 [58].

C_3N_4 to yield Matrimid®/g-C_3N_4 MMMs for improving the separation performance. Due to the presence of abundant —C—N— bonds in the g-C_3N_4 framework, it could be easily protonated by HCl, thus, resulting in surface charge modification from negative to positive. g-C_3N_4 is a laminar material with non-oxidized aromatic and aliphatic phases containing phenolic, carboxyl and oxygen epoxide groups, which make it hydrophilic in aqueous media. This behavior can be modified by treatment with oxygen plasma or hydrazine monohydrate. Use of plasma with oxygen results in dissociation to generate oxygen-containing radicals, which incorporate —OH as hydroxylamine groups, on the surface of g-C_3N_4, thus, improving its dispersibility.

In the reported work, the novel MMMS was observed to improve the gas separation by enhancing the selectivity for CO_2/CH_4 by up to 36.9% at 0.5% (mass) filler doping. With a view to further enhance the performance of the composite membrane due to the incorporation of g-C_3N_4, oxygen plasma and hydrazine monohydrate treatments were also assayed as alternatives to protonation. Hydroxylamination by oxygen plasma treatment enhanced the selectivity for CO_2/CH_4 by up to 52.2% (at 2% (mass) doping) and O_2/N_2 by up to 26.3% (at 0.5% (mass) doping). In comparison, the hydrazination process can achieve enhancements in the CO_2/CH_4 separation by up to 11.4%, but the result is lower. Chitosan (CS) modified g-C_3N_4/ZIF-8/polyethersulfone (PES) membranes were synthesized for enhanced CO_2/CH_4 separation by Abolfazl *et al.* in 2019 [59]. The layer by layer method of membrane fabrication was employed for the fabrication of ZIF-8 on PES support. The results indicated that the chitosan modified g-C_3N_4 incorporated ZIF-8 membranes exhibit superior CO_2/CH_4 ideal selectivity (24.2) as compared with the pristine ZIF-8 membrane. Due to the formation of the C—N bond between g-C_3N_4 and imidazole group of ZIF-8, the flexibility of the modified ZIF-8 membranes was observed to increase remarkably, thus, leading to a superior performance as compared to other membranes. Both theoretical and experimental results indicate that g-C_3N_4 can be used in the gas separation membranes with a superior separation effect. But, there are challenges as well. Due to the pores of g-C_3N_4, there are fewer gas molecules that can pass directly through the g-C_3N_4 layers. More separation of gas systems can be achieved by forming channels with other materials. Selectivity is the most important. Only prepare the appropriate structure, high selectivity can be required. Though the research in this field is still in infancy, the observed findings in the recent years are envisaged to result in a significant research effort in this area. In the near future, g-C_3N_4 is expected to be used in gas separation membranes at a large scale.

3.2. Pervaporation membranes for solvent dehydration

Membrane technology, with molecular level separation of substances under mild and low-cost conditions, has led to overcome serious challenges in the fields of energy, water resources and environment [60,61]. Pervaporation organic dehydration and recovery is considered as the most important application of the pervaporation technology. Ideal membrane materials generally use hydrophilic polymeric materials with rigid chains and ability to form ion–dipole interactions or hydrogen bonds with water [62]. Obviously, during application of pervaporation, there is a mutually constrained relationship between the permeability and selectivity of the membrane [25,63]. As the selectivity increases, the permeability of the components decreases, correspondingly, *i.e.*, the "trade-off" effect. One approach to overcome the "trade-off" effect of the pervaporation membranes is to prepare the organic/inorganic nano-hybrid membranes.

By adding the commonly used inorganic particles including carbon quantum dots [64], graphene and its derivatives [65,66], organometallic frameworks [67], *etc.*, the mechanical properties, thermal stability and solvent resistance of the pervaporation membrane can be enhanced. As shown in Fig. 8, compared with the per-

vaporation membranes prepared by using graphene oxide, the g-C_3N_4 pervaporation membranes demonstrate the following advantages: (1) the water nanochannels in the g-C_3N_4 membrane are stable and rigid under increasing pH conditions and pressures; (2) the N atoms in g-C_3N_4 have the possibility to form hydrogen bonds with the water molecules or other hydroxyl group-containing solvent molecules in the inter-layer, thus, leading to a unique phenomenon. In our previous study [68], it was noted that the hydroxyl groups of ethanol are closer to the surface of g-C_3N_4 than the methyl groups. This phenomenon is completely opposite to the report by Gao [69], where the methyl groups in ethanol are observed to be closer to graphene than the hydroxyl groups. The observed phenomenon is due to the lack of the hydrogen bond between ethanol and graphene surface. Therefore, the interaction between g-C_3N_4 and ethanol is stronger, which is conducive for the separation of ethanol and water. Pervaporation hybrid membranes includes polymer phase (Polyvinyl Alcohol), inorganic phase (g-C_3N_4) and polymer-inorganic interface phase. Polyvinyl alcohol (PVA) was formed on the surface of nitride by interfacial polymerization. The inorganic particles and polymer matrix exhibit four main interfacial morphologies, such as micro-phase separation, strong binding, medium binding and weak binding morphologies (See Fig. 9). The current research efforts focus on obtaining the high-performance pervaporation membranes by adjusting the interaction of the organic–inorganic interface.

By creating pores, the properties of g-C_3N_4 can be tuned to selectively allow the water molecules to pass through g-C_3N_4, while rejecting salts and dyes. For instance, Wang and co-workers developed a g-C_3N_4 membrane with artificial nanopores and self-supporting spacers by acidifying g-C_3N_4 with concentrated hydrochloric acid [69]. The pore size of the g-C_3N_4 nanosheets must be accurately tuned to allow the water molecules to pass, while rejecting the other molecules and ions. In this respect, the g-C_3N_4 membrane characterized by artificial nanopores (sizes between 1.5–3 nm) is observed to have an optimal separation performance. For the membrane thickness of 160 nm, the water flux of the g-C_3N_4 free-standing membrane was observed to be 29 $L{\cdot}m^{-2}{\cdot}h^{-1}{\cdot}bar^{-1}$ (1bar =0.1MPa), with a rejection rate of 87% (molecules larger than 3 nm). In 2015, Cao *et al.* [70] added g-C_3N_4 to sodium alginate (SA) for the first time to develop a pervaporation hybrid membrane with excellent performance. The weak binding morphology (intramolecular hydrogen bond) was observed between —NH_2 and —NH in g-C_3N_4 and —OH and COO^- in the SA chain. At 76 °C, the hybrid membrane with g-C_3N_4 content of 3% (mass) was used for the dehydration analysis employing 90% (mass) ethanol solution. The water flux of the membrane was observed to be 2469 $g{\cdot}m^{-2}{\cdot}h^{-1}$, whereas the separation factor was noted to reach up to 1653. In addition, the tensile strength of the membrane reached a maximum of 120 MPa, along with a superior thermal stability (~215 °C). Similarly, Wang *et al.* [71] fabricated the pervaporation hybrid membrane by incorporating the g-C_3N_4 nanosheets into a succinic acid-crosslinked PVA matrix. The addition of succinic acid tuned the organic–inorganic interfacial strength of the pervaporation membrane, and the hydrophilicity and heat-resistance properties of the membrane were correspondingly improved. The water flux of the g-C_3N_4 membrane was noted to be 6332 $g{\cdot}m^{-2}{\cdot}h^{-1}$, with the separation factor reaching 30.7 for 90% (mass) ethanol solution at 75 °C, as compared with 2337 $g{\cdot}m^{-2}{\cdot}h^{-1}$ and 11.2 for the cross-linked pure PVA membrane, thus, breaking the "trade-off effect" of the pervaporation membrane. Although the addition of carbon nitride enhances both membrane flux and separation factor, the dispersion and compatibility of g-C_3N_4 in the hydrophilic polymer matrices require further investigation. By performing the surface chemical modification of g-C_3N_4 to regulate the organic–inorganic interfacial microstructure in the pervaporation separation layer, a high-performance pervaporation membrane can be obtained [72]. In our earlier work, different types of g-C_3N_4 and its derivatives including g-C_3N_4 [63], hydrogen peroxide activated g-C_3N_4 (O-g-C_3N_4) and polydopamine modified g-C_3N_4 (PDA@O-g-C_3N_4) [72] were added to the cross-linked PVA for preparing the pervaporation membranes, as shown in Fig. 10. For the cross-linked PVA/O-g-C_3N_4 (CPVA-O-g-C_3N_4) hybrid membranes, the interfacial interaction between the PVA matrix and O-g-C_3N_4 nanosheets exhibits not only weak hydrogen bonding, but also rigid chemical bonding interactions. The —COOH group in O-g-C_3N_4 reacts with the OH group in the PVA chain to form an ester group, thus, confirming the role of O-g-C_3N_4 as a crosslinking agent. The permeation flux and separation factor of the CPVA-O-g-C_3N_4 membrane were noted to be 3392 $g{\cdot}m^{-2}{\cdot}h^{-1}$ and 28.9, respectively. The interaction at the polymer-inorganic interfaces in the CPVA-PDA@O-g-C_3N_4 hybrid membranes result in flexible chemical bonds, thereby leading to further grafting of PDA. The formation of the flexible chemical bonds reduces the number of non-selective interface pores in the hybrid membrane, thus, significantly improving the membrane's permeability selectivity towards aqueous ethanol solution. The permeation flux and separation factor of the CPVA-PDA@O-g-C_3N_4 membrane were noted to be 2328 $g{\cdot}m^{-2}{\cdot}h^{-1}$ and 57.9, respectively. Fig. 11 compares the separation performances of different PVA-based pervaporation membranes for ethanol dehydration.

The g-C_3N_4 composite membrane breaks the "trade-off" effect between the permeation flux and separation factor as compared to the traditional polymer membranes. Moreover, the hybrid composite pervaporation membranes exhibit high swelling resistance

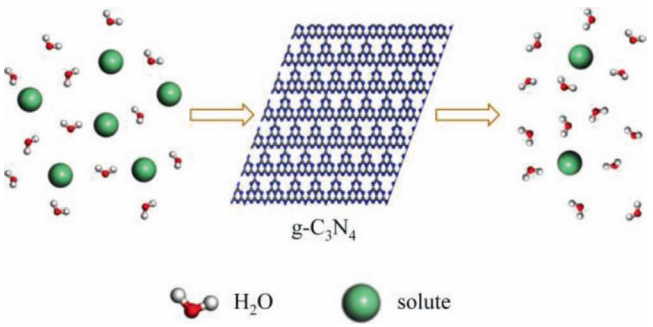

Fig. 8. Schematic diagram of solvent dehydration with g-C_3N_4.

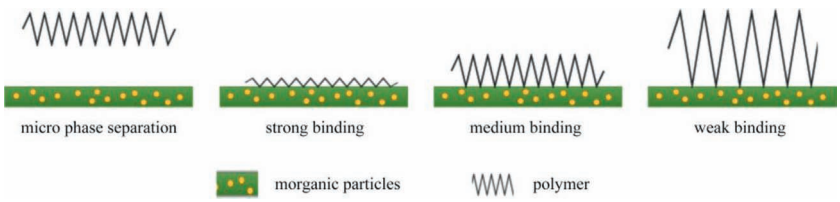

Fig. 9. Interface morphology of polymer and inorganic particles [68].

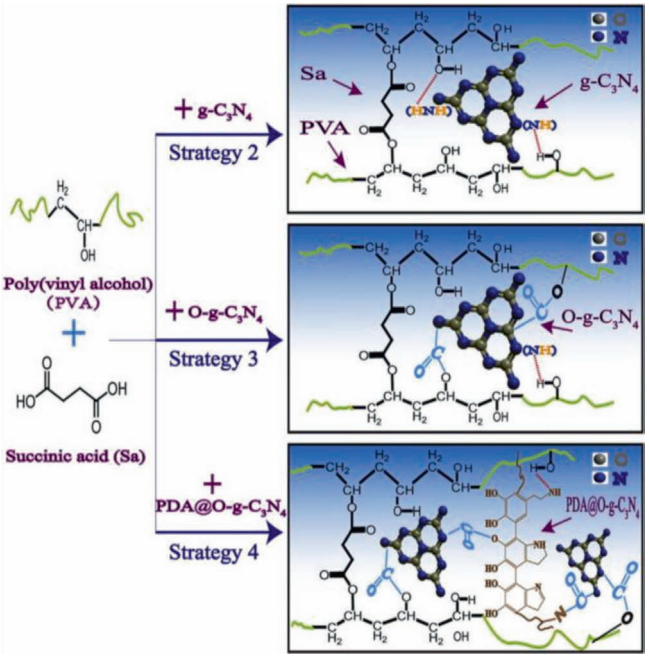

Fig. 10. The reaction mechanisms of hybrid membranes prepared with PVA, Sa and g-C_3N_4 [72].

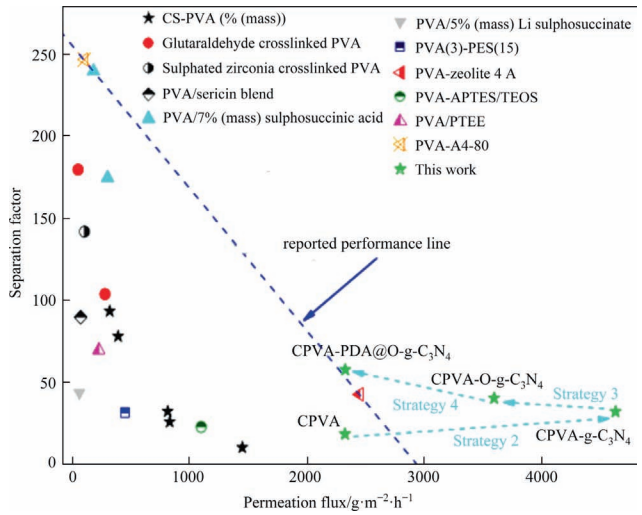

Fig. 11. Separation performance of PVA-based membranes for ethanol dehydration as reported in literature and in this work. Membranes reported in previous studies: CS-PVA (% (mass)); Glutaraldehyde crosslinked PVA, Sulphated crosslinked PVA, PVA/sericin blend, PVA/7% (mass) sulphosuccinic acid and PVA/5% (mass) Li^+ sulphosuccinate; PVA(3)-PES(15); PVA-zeolite 4A; PVA-APTES/TEOS; PVA/PTEE and PVA-A4-80 [72].

and mechanical stability. For a certain mixture, the permeation rate depends mainly on the properties of the membrane. The membrane with a high permeation rate to one component and a low permeation rate to the other component can be obtained by using appropriate membrane materials and manufacturing methods. The prepared 2D g-C_3N_4 and modified g-C_3N_4 need to be further refined and modified. High performance pervaporation membranes can be obtained by modifying g-C_3N_4.

3.3. Nanofiltration and reverse osmosis membranes for water treatment

In addition to solvent dehydration by pervaporation, g-C_3N_4 can be used for the removal of dyes and metal ions by virtue of its excellent adsorption properties and reusability. The dyes or metal ions entrapment mechanism by g-C_3N_4 is given in Fig. 12. To ensure high dye and metal ion selectivity and water permeability, the membranes must have a narrow pore size distribution, porous structure and low thickness [73–75]. It is well known that various factors, such as pore size, ion size, interaction between ions and membranes, hydration of nanopores and polymer membrane surface affect the dye and metal ion selectivity and water permeability of the membranes [76–78]. The nanopores can be generated on g-C_3N_4 to allow the channels of water, while rejecting salts and dyes [79]. The stacking of the g-C_3N_4 nanosheets as well as their hydrophobic nature result in ultra-low friction water channels for the rapid flow of water across the membrane [80]. Therefore, either g-C_3N_4 naonosheets with nanopores or stacked g-C_3N_4 can be employed for water purification application. The following sections discuss the application of g-C_3N_4 for the purpose of water purification, especially for salt rejection, water permeation capability and anti-pollution performance of membrane.

3.3.1. The improvement of salt rejection through nanoporous g-C_3N_4

Compared with the conjugated double bonds in the tri-s-triazine units in g-C_3N_4, the single bonds (N-$(C)_3$) connecting the N atoms and tri-s-triazine units are weaker, thus, enabling their easy elimination to adjust the pore size [81]. Fig. 13 presents the typical schematic of the water-salt separation process by nanoporous g-C_3N_4 membranes.

Using classical molecular dynamics, Liu and coworkers reported the permeation of water and ions through the g-C_3N_4 nanoporous membranes with different pore sizes [24]. By accurately preparing the nanopores on the g-C_3N_4 nanosheet, the g-C_3N_4 membrane was observed to sieve out the monovalent cations (at least 70%) and reject the bivalent cations (Ca^{2+}) entirely, while allowing the water molecules to penetrate. The cross-section area of the nanopores in the g-C_3N_4 nanosheet was observed to be 1.74 nm^2, 3.93 nm^2 and 6.99 nm^2, respectively, and the corresponding converted radius was 0.74 nm, 1.12 nm and 1.49 nm, respectively. In another study, Xiao *et al.* [82] prepared the 2D ultra-thin free-standing polymerized carbon nitride membranes with a unique layered structure to control the ion transport and salinity gradient energy conversion. The g-C_3N_4 free-standing membrane were negatively charged at both pH 5.8 and 10 due to unreacted amino and imine residues, thereby improving the ion selectivity at low concentrations. Although porous g-C_3N_4 demonstrates a high extent of dye reten-

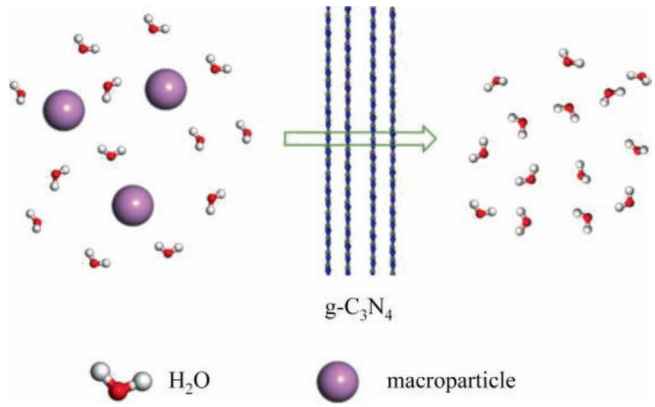

Fig. 12. Schematic diagram of particle entrapment with g-C_3N_4.

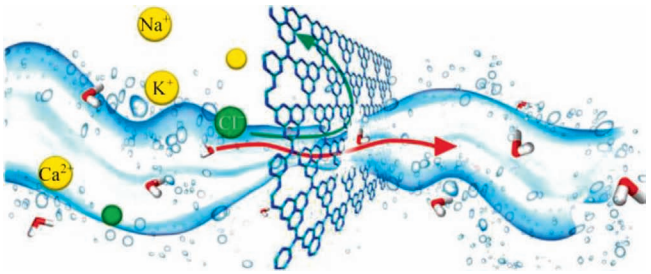

Fig. 13. The schematic of the water-salt separation process by nanoporous g-C_3N_4 membranes [24].

tion, it is still a technical challenge to generate uniformly sized nanopores on a large area of the nanosheets. In addition, the current research studies have reported that porous g-C_3N_4 separates water, ions or dyes solely by pore size. In order to further improve the salt retention and selectivity, functionalized porous g-C_3N_4 should be considered.

3.3.2. Water permeability improvement through interlayer nanochannels in g-C_3N_4

The g-C_3N_4 membranes demonstrated ultra-high water diffusion coefficients due to the ultrafast transportation of the water molecules through confinement between the g-C_3N_4 nanosheets [83]. Fig. 14 shows that the schematic of the water-salt separation process and antifouling process of the PA/CNs membrane [26]. The experimental analysis and MD simulations showed that the velocity of the water molecules through the two-layer g-C_3N_4 nanosheets was faster than *n*-hexane molecules (though the viscosity of water is larger than *n*-hexane). Meanwhile, the flux of the water molecules through the two-layer g-C_3N_4 nanosheets was noted to be similar to that of the four-layer g-C_3N_4 nanosheets. This can be attributed to the ultralow friction of the water molecules between the channels.

Wang and coworkers tuned the interlayer distance in the g-C_3N_4 membranes by inserting the anions between the g-C_3N_4 nanosheets for the selective separation of the organic species in the aqueous solution [84]. The intercalation of the sulfate anion enhanced the interlayer distance of the membrane to ~1.08 nm, thus, resulting in a water flux of 111 $L{\cdot}m^{-2}{\cdot}h^{-1}{\cdot}bar^{-1}$ (1 bar = 0.1 MPa), along with a highly enantioselective permeation towards limonene racemate with an enantiomeric excess value of 89%. In another study, Gao *et al.* [21] incorporated acidified g-C_3N_4 in the polyamide (PA) layer *via* interface polymerization. The membrane water flux was enhanced due to the formation of the nano-water channels in the PA selective layer and enhancement of the hydrophilicity at the membrane surface. The membrane incorporated with acidified g-C_3N_4 exhibited a permeate flux of 45.0 $L{\cdot}m^{-2}{\cdot}h^{-1}$ (1.8 MPa) with a NaCl rejection of 98.6%. Similarly, Abdul Aziz and coworkers fabricated the composite membranes by incorporating g-C_3N_4 or protonated g-C_3N_4 (pCN) to achieve salt separation in the aqueous solution [85]. After protonation, the g-C_3N_4 nanosheets exfoliated to pCN, thus, resulting in small size, high water dispersibility and an enhanced extent of defects on the edges of the pCN network. The high water dispersibility of pCN improved the water permeability by preventing the closure of the nanochannels. In addition, the defect-rich topology of pCN provided a shorter path for rapid water diffusion. Therefore, the acidified or protonated g-C_3N_4 enhanced the overall membrane flux.

Ye *et al.* [86] prepared the g-C_3N_4 nanofiltration membrane by doping the g-C_3N_4 nanosheets in the homogeneous dispersion of polyethylenimine (PEI) and dopamine (PDA). The g-C_3N_4 nanofiltration membrane exhibited high permeability ((28.4 ± 1.2) $L{\cdot}m^{-2}{\cdot}h^{-1}{\cdot}bar^{-1}$) due to the formation of the nano-channels in the PDA/PEI layer. Wang *et al.* [87] fabricated the g-C_3N_4-PAA hybrid membranes by incorporating polyacrylic acid (PAA) in the g-C_3N_4 nanosheets. The thickness of the membrane increased from 405 to 680 nm on enhancing the PAA content from 0.1 to 0.5 (mass ratio of PAA to the g-C_3N_4 nanosheets). Though the thickness of the membrane was enhanced, the membrane flux did not decrease (from 117 to 143.1 $L{\cdot}m^{-2}{\cdot}h^{-1}$) due to the larger nanochannels formed on incorporating PAA. By adding the nanoparticles of different dimensions, the surface roughness and microstructure of the membranes could be modified, thus, enhancing the pure water flux of the membranes. In another study, Liu *et al.* [88] transferred g-C_3N_4, halloysite nanotubes and piperazine monomers in the PSF substrate by vacuum filtration, followed by polymerization with trimesoyl chloride by interfacial polymerization to prepare the thin film nanocomposite (TFN) membranes. The nanomaterial addition enhanced the surface roughness and hydrophilicity of the TFN membranes. As a result, the water flux of the TFN membranes was observed to improve further (205 $L{\cdot}m^{-2}{\cdot}h^{-1}{\cdot}MPa^{-1}$). Table 3 presents the desalination parameters of various g-C_3N_4 based nanofiltration membranes.

In summary, by tuning the membrane channels and pores on g-C_3N_4, the flux and selectivity of the membranes could be effectively controlled. Nanofiltration and reverse osmosis membranes have high ion retention rate. Compared with the graphene membrane, the charge distribution of the g-C_3N_4 membrane exhibited a significant impact on the penetration of ions through the nanopores and nanochannels. So, It has a lot of limitations in ion intercept for g-C_3N_4. The charge distribution of the material should be changed to achieve a high ion retention rate.

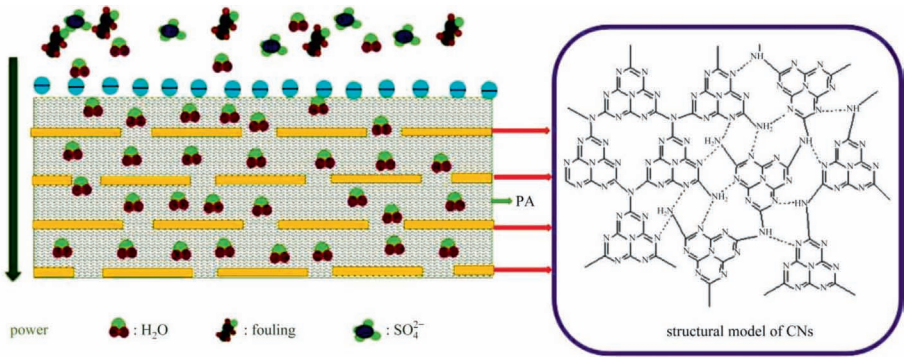

Fig. 14. The schematic of the water-salt separation process and antifouling process of the PA/CNs membrane [26].

Table 3
Comparison of divalent and monovalent rejection as well as water permeation abilities of various g-C_3N_4 incorporated membranes (1 bar = 0.1 MPa)

Membrane material	Solute	Rejection	Permeability/water flux	Ref.
g-C_3N_4/PAN	$MgSO_4$	30.79%	7.1 $L{\cdot}m^{-2}{\cdot}h^{-1}{\cdot}bar^{-1}$	[89]
g-C_3N_4/PAN	NaCl	18.96%	5.2 $L{\cdot}m^{-2}{\cdot}h^{-1}{\cdot}bar^{-1}$	[89]
g-C_3N_4/PAN	Methyl blue	99.83%	11.7 $L{\cdot}m^{-2}{\cdot}h^{-1}{\cdot}bar^{-1}$	[89]
PDA/PEI/g-C_3N_4	NaCl	2.9%	28.4 $L{\cdot}m^{-2}{\cdot}h^{-1}{\cdot}bar^{-1}$	[90]
PDA/PEI/g-C_3N_4	Na_2SO_4	7.6%	28.4 $L{\cdot}m^{-2}{\cdot}h^{-1}{\cdot}bar^{-1}$	[90]
PDA/PEI/g-C_3N_4	Reactive orange 16	98.7%	20.6 $L{\cdot}m^{-2}{\cdot}h^{-1}{\cdot}bar^{-1}$	[90]
PDA/PEI/g-C_3N_4	Reactive orange 1	99.1%	20.2 $L{\cdot}m^{-2}{\cdot}h^{-1}{\cdot}bar^{-1}$	[90]
PDA/PEI/g-C_3N_4	reactive blue 19	99.3%	20.4 $L{\cdot}m^{-2}{\cdot}h^{-1}{\cdot}bar^{-1}$	[90]
g-C_3N_4/HNT/PSF	Na_2SO_4	94.5%	20.5 $L{\cdot}m^{-2}{\cdot}h^{-1}{\cdot}bar^{-1}$	[91]
g-C_3N_4/HNT/PSF	$MgSO_4$	91.3%	20.5 $L{\cdot}m^{-2}{\cdot}h^{-1}{\cdot}bar^{-1}$	[91]
g-C_3N_4/polyamide	Na_2SO_4	84.0%	37.6 $L{\cdot}m^{-2}{\cdot}h^{-1}$ (2 bar)	[30]
Gly-GO/g-C_3N_4	Rhodamine B	77.7%	42.9 $L{\cdot}m^{-2}{\cdot}h^{-1}{\cdot}bar^{-1}$	[92]
Gly-GO/g-C_3N_4	Alcian blue	89.5%	56.1 $L{\cdot}m^{-2}{\cdot}h^{-1}{\cdot}bar^{-1}$	[92]
Gly-GO/g-C_3N_4	Methyl blue	90%	25.8 $L{\cdot}m^{-2}{\cdot}h^{-1}{\cdot}bar^{-1}$	[92]
g-C_3N_4/HNTs	NaCl	93%	2.17 $L{\cdot}m^{-2}{\cdot}h^{-1}{\cdot}bar^{-1}$	[93]
g-C_3N_4/PAA-0.1	Evans blue	83%	117 $L{\cdot}m^{-2}{\cdot}h^{-1}$ (1 bar)	[94]
aCN/PA	NaCl	98.6%	45.0 $L{\cdot}m^{-2}{\cdot}h^{-1}$ (18 bar)	[95]

3.4. Ion exchange membranes

The ion exchange membranes, as a kind of polymer films, have selective transmissibility towards ions. The major performance indicators include ion exchange capacity (IEC), conductivity and selective transmittance [93–95]. As shown in Fig. 15, g-C_3N_4 is resistant to strong acids as well as alkalinity and produces electron-hole pairs swiftly [94,96]. Therefore, g-C_3N_4 is added to the ion exchange membranes to improve their performance [97]. There are a large number of amino groups on the surface of g-C_3N_4, so g-C_3N_4 can be combined with other materials to form ion transport channels. Simultaneously, due to the characteristics of g-C_3N_4, the structural properties of the ion exchange membranes are also improved [93].

Hybrid membranes (SPEEK/g-C_3N_4) composed of sulfonated poly (ether ether ketone) (SPEEK) and g-C_3N_4 were fabricated by

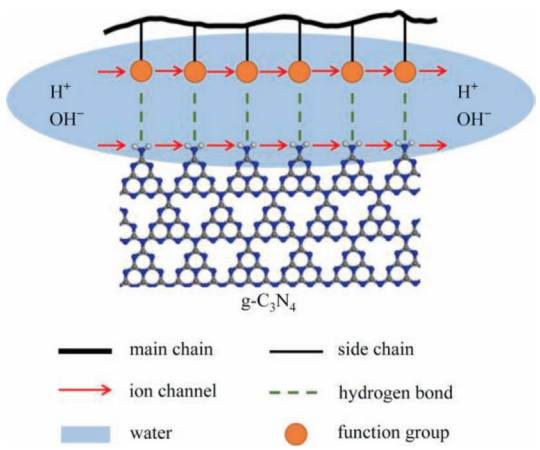

Fig. 15. Schematic diagram of ion transport mechanism with g-C_3N_4.

Niu *et al.* in 2016 by employing a solution-casting method for vanadium redox flow battery (VRB) [23]. The authors observed that the physicochemical properties, such as swelling ratio (SR), ion exchange capacity, proton conductivity and vanadium ion permeability, changed with the content of the g-C_3N_4 nanosheets.

The structure–property performance of the SPEEK/g-C_3N_4 hybrid membranes was analyzed, whereby the physicochemical properties such as swelling ratio, water uptake (WU), electrolyte uptake (EU), proton conductivity (δ) and vanadium ion permeability were studied as a function of the content of the g-C_3N_4 nanosheets. The desired ratio of g-C_3N_4 in the SPEEK/g-C_3N_4 hybrid membranes varied from 0.5 to 2.5% (0.5%, 1%, 1.5%, 2% and 2.5% (mass)) (see Table 4).

The results indicated that the interfacial interaction was regulated by the incorporated g-C_3N_4 nanosheets, which effectively controlled the ion selectivity, vanadium ion permeation and structure stability of the hybrid membranes. The mechanisms for the proton transport and vanadium ion permeation in the hybrid membrane were proposed in Fig. 16. The acid-base pairs and unique nanoporous structure of the g-C_3N_4 nanosheets promoted the proton transport and restricted the vanadium ion permeation. In another similar study, Wang *et al.* [96] prepared a composite membrane in 2017 by adding oxidized g-C_3N_4 (OCN). The bulk g-C_3N_4 was acid-treated by using a mixture of concentrated sulfuric acid and nitric acid to produce OCN at room temperature. A large number of amino groups on the surface of the g-C_3N_4 were oxidized by the strong acids and correspondingly replaced by the hydroxyl groups. The permeability and selectivity of vanadium were tested to ascertain the properties of the membrane (see Table 5).

The uniformly dispersed OCN powder in the SPEEK matrix not only decreased the diffusion of the vanadium ions significantly, but also enhanced the ion selectivity of the composite membrane. Meanwhile, a superior cycling stability of the hybrid membrane was obtained. Ion exchange membranes are most widely used in

Table 4
WU, SR, EU, IEC and σ of Nafion 117, SPEEK and SPEEK/g-C_3N_4 hybrid membranes [23].

Samples	WU/%	EU/%	SR/%	IEC/$mmol{\cdot}g^{-1}$	σ/$mS{\cdot}cm^{-1}$
Nafion 117	21.1 ± 0.3	19.6 ± 0.2	28.9 ± 0.4	0.88 ± 0.01	11.7 ± 0.3
SPEEK	32.6 ± 0.4	40.9 ± 0.5	13.7 ± 0.2	1.75 ± 0.01	6.6 ± 0.3
0.5%	19.1 ± 0.1	19.3 ± 0.4	5.7 ± 0.3	0.81 ± 0.01	5.6 ± 0.3
1.0%	19.5 ± 0.3	20.7 ± 0.4	5.2 ± 0.3	0.83 ± 0.01	6.0 ± 0.3
1.5%	20.7 ± 0.2	21.8 ± 0.5	5.7 ± 0.5	0.86 ± 0.01	7.9 ± 0.3
2.0%	28.6 ± 0.4	22.7 ± 0.3	5.6 ± 0.1	0.95 ± 0.01	12.3 ± 0.3
2.5%	27.5 ± 0.5	20.9 ± 0.4	5.7 ± 0.2	0.79 ± 0.01	8.2 ± 0.3

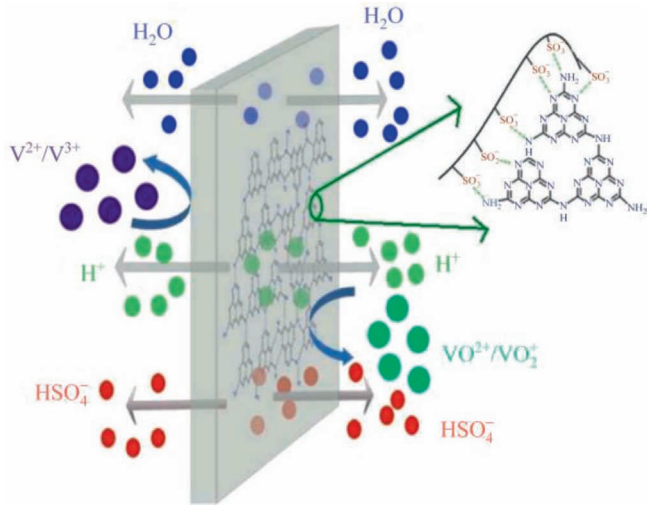

Fig. 16. Proposed mechanism for the proton transport and vanadium ion permeation in the hybrid membrane [23].

batteries. In this respect, the use of g-C_3N_4 to modify the ion exchange membrane in batteries to improve their performance has attracted a significant research attention. A series of proton exchange membranes have been fabricated by Liu *et al.* in 2019 with the g-C_3N_4 nanosheets as nanofiller and sulfonated polysulfone (SPSF) as membrane matrix by employing the simple solution-casting method [97] (see Table 6).

The ion selectivity, permeability, proton conductivity and mechanical properties were observed to be significantly enhanced on incorporation of g-C_3N_4 in the SPSF matrix. SPSF/g-C_3N_4-1 exhibited the highest ion selectivity and lowest permeability as compared to Nafion 117 and pristine SPSF. An optimal balance between selectivity and permeability of the high-performance acid-base composite membranes could, thus, be promoted for vanadium redox flow batteries. In summary, by virtue of its physical and chemical properties, g-C_3N_4 improves the selectivity of the ion exchange membranes, while maintaining an optimal permeability. Further, the conductivity and IEC can be improved, along with the cycle time and service life of the membranes. The amino group on the surface of g-C_3N_4 is the key to the application of ion exchange membranes. Ion transport channels can be obtained when the g-C_3N_4 combined with other materials.

3.5. Catalytic separation membranes

During the actual operation, especially with the organic components, the surface of the membrane absorbs a large number of organic substances after a period of use, thus, resulting in the membrane pollution and decreased flux, thus, weakening the separation effect [98,99]. To overcome this issue, the substances are usually added to the membrane to reduce the adsorption of the organic matter on the surface in order to improve the anti-pollution ability of the membrane [98–101].

As a novel non-metallic photocatalytic material, g-C_3N_4 exhibits a wide range of absorption spectrum and can play a photocatalytic role in the ordinary visible light without the need of the ultraviolet light [102–104]. As shown in Fig. 17, g-C_3N_4 effectively activates the molecular oxygen and produces the superoxide radicals, which can be used for the photocatalytic transformation of the organic functional groups and photocatalytic degradation of the organic pollutants. Due to its photocatalytic properties, g-C_3N_4 is added to catalyze the decomposition of the organic components on the membrane surface in Fig. 18 [105]. In 2016, Zhao *et al.* [106] assembled the graphitic carbon nitride nanosheet/reduced graphene oxide (g-C_3N_4 NS/RGO) composite based photocatalyst on a commercial cellulose acetate (CA) membrane by vacuum filtra-

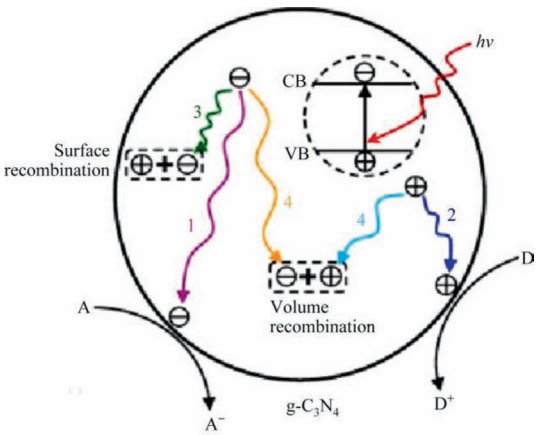

Fig. 17. Schematic illustration of the photo excited electron – hole pairs in g-C_3N_4 with possible decay pathways. A and D denote electron acceptor and electron donor, respectively [102].

Table 5
The physicochemical properties of Nafion 117, pure SPEEK and composite membranes [96].

Sample	Water uptake/%	Swelling ration/%	IEC/mmol·g^{-1}	Proton conductivity/S·cm^{-1}	VO^{2+} permeability/10^{-7}cm^2 ·min^{-1}	Selectivity/10^4S· min·cm^{-3}
Nafion 117	28.5	16.3	0.91	0.097	36.50	2.66
SPEEK	26.7	18.1	1.49	0.053	15.60	3.40
S/OCN-0.5	34.5	19.2	1.52	0.055	10.00	5.50
S/OCN-1	48.2	19.3	1.56	0.060	9.09	6.60
S/OCN-2	36.4	16.3	1.49	0.048	7.70	6.23

Table 6
WU, SR, IEC, and σ of Nafion 117, SPSF and SPSF/g-C_3N_4 composite membranes [97].

Samples	WU/%	EU/%	SR/%	IEC/mmol·g^{-1}	σ/mS·cm^{-1}
Nafion 117	186 ± 1	0.88 ± 0.01	21.1 ± 0.3	28.9 ± 0.3	26.8 ± 0.3
SPSF	81 ± 1	1.26 ± 0.01	24.5 ± 0.2	7.5 ± 0.3	13.5 ± 0.3
0.5%	86 ± 1	1.15 ± 0.01	20.1 ± 0.4	6.3 ± 0.1	14.8 ± 0.2
1.0%	85 ± 1	1.11 ± 0.01	19.9 ± 0.4	5.8 ± 0.1	15.2 ± 0.2
1.5%	84 ± 1	1.08 ± 0.01	19.5 ± 0.3	5.5 ± 0.1	16.9 ± 0.2
2.0%	86 ± 1	1.03 ± 0.01	17.6 ± 0.3	5.4 ± 0.1	17.2 ± 0.3

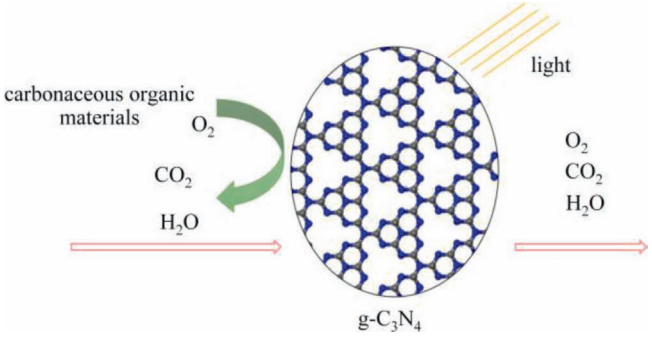

Fig. 18. Schematic diagram of catalytic separation membrane prepared with g-C_3N_4.

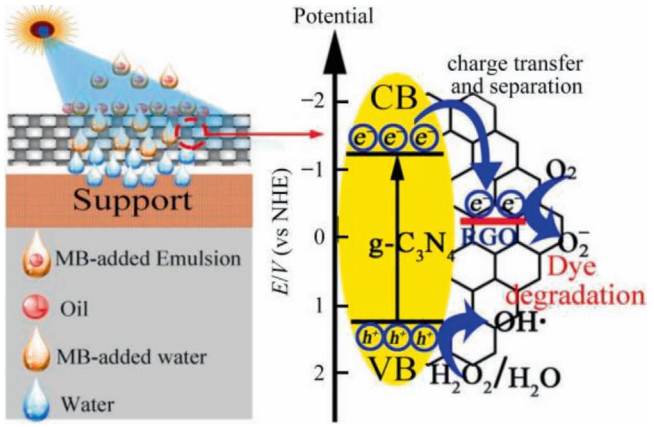

Fig. 20. The schematic illustration of oil/water separation and photocatalytic degradation process in the composite membrane [27].

tion and high-pressure processing for water treatment. The photocatalytic efficiency of the g-C_3N_4 NS/RGO composite with different RGO contents was evaluated through the degradation of Rhodamine B (RhB) in a quartz reactor. The g-C_3N_4 NS/RGO/CA composite photocatalytic membrane exhibited high efficiency for the removal of the organic contaminants in the integrated process of filtration and visible light photocatalysis. The membrane was observed to demonstrate antibacterial properties as well. In a similar study, a RGO/PDA/g-C_3N_4-CA composite membrane was prepared by Li *et al.* in 2017 for the catalytic decomposition and oil-in-water emulsion separation [27]. The synthesis of the RGO/PDA/g-C_3N_4 composites is shown in Fig. 19. The RGO/PDA/g-C_3N_4 membrane was fabricated by carrying out the dopamine modification, followed by the assembly of the RGO/PDA/g-C_3N_4 composite on the surface of commercial CA membrane.

The photocatalytic efficiency of the free-standing RGO/PDA/g-C_3N_4 composite membranes with different g-C_3N_4 content were evaluated through the degradation of methylene blue (MB). The oil/water emulsions were prepared by mixing the diesel oil and water. The oil/water emulsion and MB aqueous solution containing H_2O_2 were filtered through the RGO/PDA/g-C_3N_4/CA composite membrane using a vacuum filtration setup and visible-light irradiation. The oil/water separation and photocatalytic degradation process in the composite membrane are shown in Fig. 20. The novel RGO/PDA/g-C_3N_4 composite membranes with flow-through catalytic degradation of the soluble organic dye molecules and oil/water emulsion separation were successfully prepared by using the vacuum filtration method. The authors attributed the excellent performance to the compact 2D-2D structure of RGO and g-C3N4 with dopamine modification. RGO with superior electron transport properties efficiency separated the photoelectrons by g-C_3N_4 production under light illumination. As shown in Fig. 21, a highly efficient oilfield produced water treatment, the photocatalytic

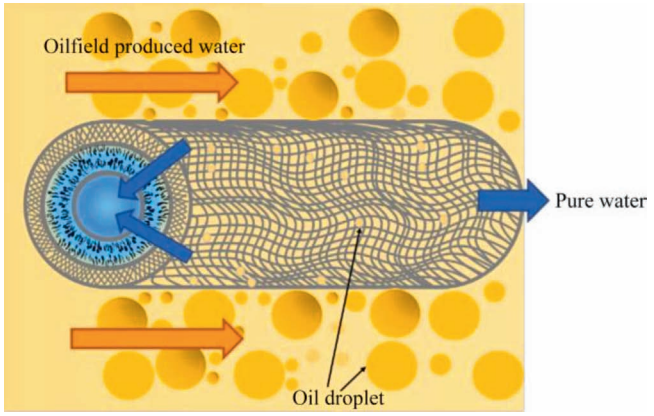

Fig. 21. Crossflow filtration of OPW using NF-nsGCN/Al_2O_3 membrane [107].

nanofiber-coated alumina hollow fiber membranes were prepared by Alias *et al.* [107] in 2018. The membranes were fabricated by coating the polyacrylonitrile (PAN) nanofibers incorporated with photocatalytic g-C_3N_4 on Al_2O_3 hollow fiber membrane. The highly porous coating consisting of smooth hydrophilic nanofibers facilitated the water permeation, with the coating effectively capturing the oil droplets in its opening, thus, resulting in an effective rejection efficiency against oil contaminants. In another study, GCN-embedded PAN nanofibers were electrospuned on top of the Al_2O_3 hollow fiber membrane surface using direct electrospinning technique. The permeability and pollution resistance of the mem-

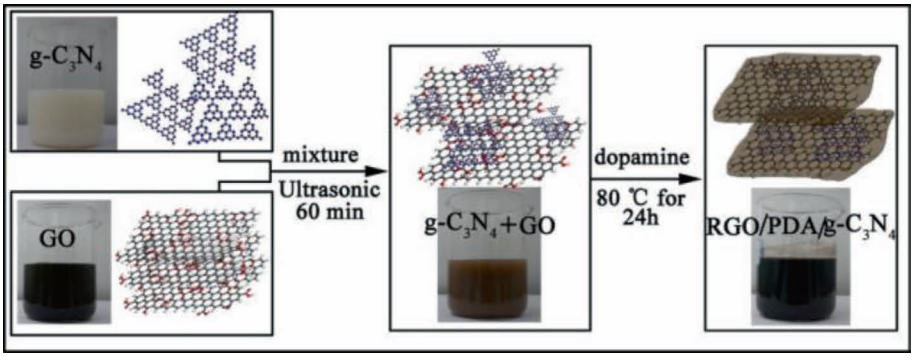

Fig. 19. Schematic of the synthesis of the RGO/PDA/g-C_3N_4 composites [27].

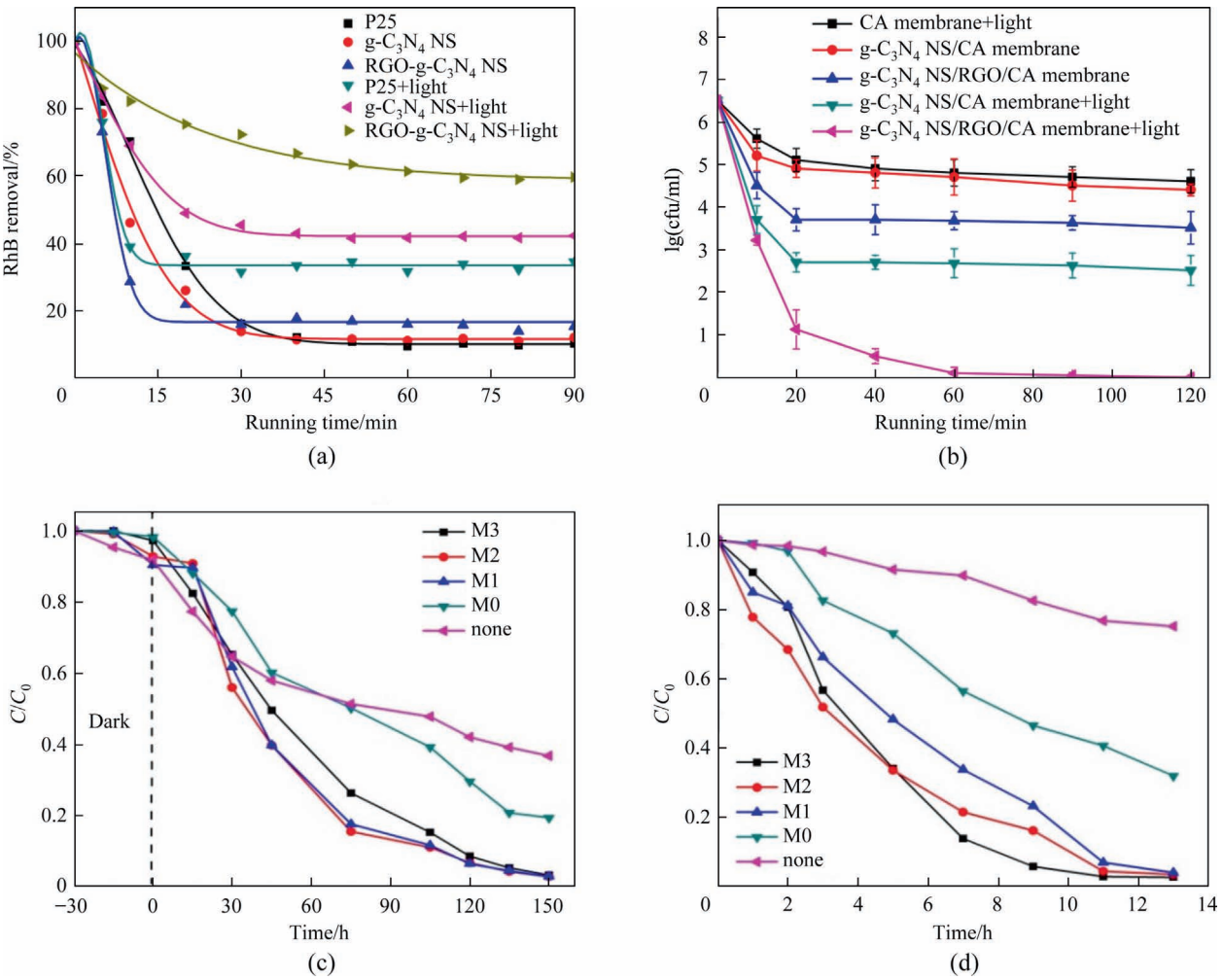

Fig. 22. (a) Removal of RhB by different membranes under diverse conditions [106]; (b) *E. coli* removal under different conditions. Photocatalytic degradation of MB by free standing membrane without H_2O_2 (c) and with H_2O_2 (d) under visible-light irradiation [27].

brane were investigated for the treatment of oilfield produced water (OPW).

The crossflow filtration using the fabricated membranes demonstrated a significant improvement in the pure water flux, OPW permeate flux and oil rejection percentage as compared to the bare Al_2O_3 membrane. Sparse mesh structure, high water affinity and smooth nanofiber morphology were observed to be the key parameters for the nanofiber coatings leading to significantly improved membrane performance. The photodegradation ability of the NF-nsGCN nanofibers enabled the coating to degrade the captured oil contaminants under UV irradiation, which helped to maintain the high permeate flux and rejection in the repeated filtration system.

Overall, the literature studies confirm that the excellent photocatalytic performance of g-C_3N_4 has a significant impact on the anti-pollution (Fig. 22(a), (b)) and catalytic decomposition abilities (Fig. 22(c), (d)) of the membrane. When g-C_3N_4 is applied to catalytic separation membranes, catalytic performance of g-C_3N_4 will be affected. The key to this research is how to balance these two properties.

4. Conclusions

The motivation for this review originates from the abundant research studies and extensive developments in the membrane technology during the last decade. Specifically, the 2D membranes from g-C_3N_4 are focused in this review due to their strong potential of commercial application, though only a few reports are currently available on the application of g-C_3N_4 in membranes. For this purpose, a few prominent C_3N_4 systems were chosen and analyzed in detail. g-C_3N_4 exhibits the characteristics of visible light catalysis and unique 2D microstructure. So, by incorporating g-C_3N_4 to membranes, the performance of the membranes is expected to be significantly improved. However, the addition of carbon nitride was not particularly effective for all membranes. Comparing recent studies, we think that g-C_3N_4 is more suitable for nanofiltration membranes or reverse osmosis membranes. Because g-C_3N_4 has a higher retention rate for ions and macromolecules than other particles. At the same time, the catalytic performance of the bulk g-C_3N_4 is not good and can be improved when the g-C_3N_4 was treated, such as g-C_3N_4 nanosheets. Nevertheless, the catalytic performance of g-C_3N_4 is lower than that of traditional metal catalysts. In terms of materials, the performance of bulk g-C_3N_4 is not particularly outstanding and must be modified to give full play to its superior performance. Green and environmental protection is now the trend of research. As a stable, non-toxic and pollution-free material, g-C_3N_4 will be applied in more fields and scenarios in the future not only membranes. The preparation of high performance g-C_3N_4 is a research hotspot in the future.

Declaration of Competing Interest

The authors declare that they have no known competing financial interests or personal relationships that could have appeared to influence the work reported in this paper.

Acknowledgements

The authors are grateful for the financial support of the National Natural Science Foundation of China (No. 21878118), Natural Science Foundation of the Jiangsu Higher Education Institutions of China (21KJA530002, 19KJA150009), Natural Science Foundation of Jiangsu Province (BK20211368) and Jiangsu Province Qing Lan Project for the Young Academic Leaders (Meisheng Li, 2021).

References

[1] K.K. Sirkar, Membrane separation technologies: Current developments, *Chem. Eng. Commun.* 157 (1) (1997) 145–184.
[2] R.W. Baker, Research needs in the membrane separation industry: Looking back, looking forward, *J. Membr. Sci.* 362 (1–2) (2010) 134–136.
[3] T.Y. Cath, A.E. Childress, M. Elimelech, Forward osmosis: Principles, applications, and recent developments, *J. Membr. Sci.* 281 (1–2) (2006) 70–87.
[4] M.Y. DeZoysa, A.H. Chon, L.M. Korst, A. Llanes, R.H. Chmait, Membrane separation and perinatal outcomes after laser treatment for twin-twin transfusion syndrome, *Fetal Diagn. Ther.* 47 (4) (2020) 1–8.
[5] Z. Feng, X.D. Chen, X.D. Wu, M.J. Zhang, Formation of biological condensates via phase separation: Characteristics, analytical methods, and physiological implications, *J. Biol. Chem.* 294 (40) (2019) 14823–14835.
[6] Y.Q. Yang, K. Goh, P. Weerachanchai, T.H. Bae, 3D covalent organic framework for morphologically induced high-performance membranes with strong resistance toward physical aging, *J. Membr. Sci.* 574 (2019) 235–242.
[7] K.L. Wang, X.R. Liu, Y. Tan, W. Zhang, S.F. Zhang, J.Z. Li, Two-dimensional membrane and three-dimensional bulk aerogel materials *via* top-down wood nanotechnology for multibehavioral and reusable oil/water separation, *Chem. Eng. J.* 371 (2019) 769–780.
[8] J.D. Shao, H.H. Xie, H.Y. Wang, W.H. Zhou, Q. Luo, X.F. Yu, P.K. Chu, 2D material-based nanofibrous membrane for photothermal cancer therapy, *ACS Appl Mater Int.* 10 (1) (2018) 1155–1163.
[9] W. Liu, D.J. Wang, R.A. Soomro, F. Fu, N. Qiao, Y. Yu, R. Wang, B. Xu, Ceramic supported attapulgite-graphene oxide composite membrane for efficient removal of heavy metal contamination, *J. Membr. Sci.* 591 (2019) 117323.
[10] K. Varoon, X. Zhang, B. Elyassi, D.D. Brewer, M. Gettel, S. Kumar, J.A. Lee, S. Maheshwari, A. Mittal, C.Y. Sung, M. Cococcioni, L.F. Francis, A.V. McCormick, K.A. Mkhoyan, M. Tsapatsis, Dispersible exfoliated zeolite nanosheets and their application as a selective membrane, *Science* 334 (6052) (2011) 72–75.
[11] V. Dincă, A. Mocanu, G. Isopencu, C. Busuioc, S. Brajnicov, A. Vlad, M. Icriverzi, A. Roseanu, M. Dinescu, M. Stroescu, A. Stoica-Guzun, M. Suchea, Biocompatible pure ZnO nanoparticles-3D bacterial cellulose biointerfaces with antibacterial properties, *Arab. J. Chem.* 13 (1) (2020) 3521–3533.
[12] J. Yu, Y. Zhang, J.H. Chen, L.L. Cui, W.H. Jing, Solvothermal-induced assembly of 2D–2D rGO-TiO_2 nanocomposite for the construction of nanochannel membrane, *J. Membr. Sci.* 600 (2020) 117870.
[13] K.C. Guan, D. Zhao, M.C. Zhang, J. Shen, G.Y. Zhou, G.P. Liu, W.Q. Jin, 3D nanoporous crystals enabled 2D channels in graphene membrane with enhanced water purification performance, *J. Membr. Sci.* 542 (2017) 41–51.
[14] K. Celebi, J. Buchheim, R.M. Wyss, A. Droudian, P. Gasser, I. Shorubalko, J.I. Kye, C. Lee, H.G. Park, Ultimate permeation across atomically thin porous graphene, *Science* 344 (6181) (2014) 289–292.
[15] B. Min, S.W. Yang, A. Korde, Y.H. Kwon, C.W. Jones, S. Nair, Continuous zeolite MFI membranes fabricated from 2D MFI nanosheets on ceramic hollow fibers, *Angew. Chem. Int. Ed.* 131 (24) (2019) 8285–8289.
[16] Y. Wang, L.J. Li, L.T. Yan, X. Gu, P.C. Dai, D.D. Liu, J.G. Bell, G.M. Zhao, X.B. Zhao, K.M. Thomas, Bottom-up fabrication of ultrathin 2D Zr metal-organic framework nanosheets through a facile continuous microdroplet flow reaction, *Chem. Mater.* 30 (9) (2018) 3048–3059.
[17] L. Ding, Y.Y. Wei, Y.J. Wang, H.B. Chen, J. Caro, H.H. Wang, A two-dimensional lamellar membrane: MXene nanosheet stacks, *Angew. Chem. Int. Ed.* 129 (7) (2017) 1851–1855.
[18] Y. Wang, X.C. Wang, M. Antonietti, Polymeric graphitic carbon nitride as a heterogeneous organocatalyst: from photochemistry to multipurpose catalysis to sustainable chemistry, *Angew. Chem. Int. Ed.* 51 (1) (2012) 68–89.
[19] B. Ou, J.X. Wang, Y. Wu, S. Zhao, Z. Wang, Efficient removal of Cr (VI) by magnetic and recyclable calcined CoFe-LDH/g-C_3N_4 *via* the synergy of adsorption and photocatalysis under visible light, *Chem. Eng. J.* 380 (2020) 122600.
[20] K.T. Cao, Z.Y. Jiang, X.S. Zhang, Y.M. Zhang, J. Zhao, R.S. Xing, S. Yang, C.Y. Gao, F.S. Pan, Highly water-selective hybrid membrane by incorporating g-C3N4 nanosheets into polymer matrix, *J. Membr. Sci.* 490 (2015) 72–83.
[21] X. Gao, Y.M. Li, X.L. Yang, Y.N. Shang, Y. Wang, B.Y. Gao, Z.N. Wang, Highly permeable and antifouling reverse osmosis membranes with acidified graphitic carbon nitride nanosheets as nanofillers, *J. Mater. Chem. A* 5 (37) (2017) 19875–19883.
[22] F. Li, Y.Y. Qu, M.W. Zhao, Efficient helium separation of graphitic carbon nitride membrane, *Carbon* 95 (2015) 51–57.
[23] R.T. Niu, L.Q. Kong, L.Y. Zheng, H.X. Wang, H.F. Shi, Novel graphitic carbon nitride nanosheets/sulfonated poly(ether ether ketone) acid-base hybrid membrane for vanadium redox flow battery, *J. Membr. Sci.* 525 (2017) 220–228.
[24] Y.C. Liu, D.Q. Xie, M.R. Song, L.Z. Jiang, G. Fu, L. Liu, J.Y. Li, Water desalination across multilayer graphitic carbon nitride membrane: Insights from non-equilibrium molecular dynamics simulations, *Carbon* 140 (2018) 131–138.
[25] R.L.G. Lecaros, M.E. Bismonte, B.T. DomaJr, W.S. HungJr, C.C. HuJr, H.A. TsaiJr, S.H. HuangJr, K.R. LeeJr, J.Y. LaiJr, Alcohol dehydration performance of pervaporation composite membranes with reduced graphene oxide and graphene quantum dots homostructured filler, *Carbon* 162 (2020) 318–327.
[26] J.X. Chen, Z.Y. Li, C.B. Wang, H. Wu, G. Liu, Synthesis and characterization of g-C3N4 nanosheet modified polyamide nanofiltration membranes with good permeation and antifouling properties, *RSC Adv.* 6 (113) (2016) 112148–112157.
[27] F. Li, Z.X. Yu, H. Shi, Q.B. Yang, Q. Chen, Y. Pan, G.Y. Zeng, L. Yan, A Mussel-inspired method to fabricate reduced graphene oxide/g-C3N4 composites membranes for catalytic decomposition and oil-in-water emulsion separation, *Chem. Eng. J.* 322 (2017) 33–45.
[28] D.M. Teter, R.J. Hemley, Low-compressibility carbon nitrides, *Science* 271 (5245) (1996) 53–55.
[29] H. Montigaud, B. Tanguy, G. Demazeau, I. Alves, S. Courjault, C3N4: Dream or reality? Solvothermal synthesis as macroscopic samples of the C3N4 graphitic form, *J. Mater. Sci.* 35 (10) (2000) 2547–2552.
[30] E.G. Gillan, Synthesis of nitrogen-rich carbon nitride networks from an energetic molecular azide precursor, *Chem. Mater.* 12 (12) (2000) 3906–3912.
[31] E. Kroke, M. Schwarz, E. Horath-Bordon, P. Kroll, B. Noll, A.D. Norman, Tri-s-triazine derivatives. Part I. From trichloro-tri-s-triazine to graphitic C_3N_4 structures, *New J. Chem.* 26 (5) (2002) 508–512.
[32] H.Z. Zhao, X.L. Chen, C.C. Jia, T. Zhou, X.H. Qu, J.K. Jian, Y.P. Xu, T. Zhou, A facile mechanochemical way to prepare g-C_3N_4, *Mater. Sci. Eng., B* 122 (2) (2005) 90–93.
[33] Y.J. Wen, D. Qu, L. An, X. Gao, W.S. Jiang, D.D. Wu, D.X. Yang, Z.C. Sun, Defective g-C3N4 prepared by the $NaBH_4$ reduction for high-performance H_2 production, *ACS Sustain. Chem. Eng.* 7 (2) (2019) 2343–2349.
[34] L. Jia, X.X. Cheng, X.N. Wang, H. Cai, P. He, J.Y. Ma, L.L. Li, Y. Ding, X.X. Fan, Large-scale preparation of g-C_3N_4 porous nanotubes with enhanced photocatalytic activity by using salicylic acid and melamine, *Ind. Eng. Chem. Res.* 59 (3) (2020) 1065–1072.
[35] H. Miao, G.W. Zhang, X.Y. Hu, J.L. Mu, T.X. Han, J. Fan, C.J. Zhu, L.X. Song, J.T. Bai, X. Hou, A novel strategy to prepare 2D g-C_3N_4 nanosheets and their photoelectrochemical properties, *J. Alloy. Compd.* 690 (2017) 669–676.
[36] J. Lu, Y. Wang, J.F. Huang, L.Y. Cao, J.Y. Li, G.J. Hai, Z. Bai, One-step synthesis of g-C_3N_{VV} hierarchical porous structure nanosheets with dramatic ultraviolet light photocatalytic activity, *Mater. Sci. Eng., B* 214 (2016) 19–25.
[37] C. Li, C.B. Cao, H.S. Zhu, Graphitic carbon nitride thin films deposited by electrodeposition, *Mater. Lett.* 58 (12–13) (2004) 1903–1906.
[38] A. Thomas, A. Fischer, F. Goettmann, M. Antonietti, J.O. Müller, R. Schlögl, J.M. Carlsson, Graphitic carbon nitride materials: Variation of structure and morphology and their use as metal-free catalysts, *J. Mater. Chem.* 18 (41) (2008) 4893–4908.
[39] Y.H. Wang, X.H. Pan, Q.H. Zheng, Z. Lin, F. Huang, Al-doped ZnO thin film enhancing the photo-catalytic bactericidal performance on the (1 0 0) plane of ZnO single crystal, *Catal. Today* 224 (2014) 188–192.
[40] Y.P. Wang, X.Y. Xia, J.W. Zhu, Y. Li, X. Wang, X.D. Hu, Catalytic activity of nanometer-sized CuO/Fe_2O_3 on thermal decompositon of AP and combustion of AP-based propellant, *Combust. Sci. Technol.* 183 (2) (2010) 154–162.
[41] S.G. Kumar, L.G. Devi, Review on modified TiO_2 photocatalysis under UV/visible light: selected results and related mechanisms on interfacial charge carrier transfer dynamics, *J. Phys. Chem. A* 115 (46) (2011) 13211–13241.
[42] A. Kay, I. Cesar, M. Grätzel, New benchmark for water photooxidation by nanostructured α-Fe_2O_3 films, *J. Am. Chem. Soc.* 128 (49) (2006) 15714–15721.
[43] S. Cao, J. Low, J. Yu, M. Jaroniec, Polymeric photocatalysts based on graphitic carbon nitride, *Adv. Mater.* 27 (13) (2015) 2150–2176.
[44] W.J. Ong, L.L. Tan, Y.H. Ng, S.T. Yong, S.P. Chai, Graphitic Carbon Nitride (g-C3N4)-based photocatalysts for artificial photosynthesis and environmental remediation: are we a step closer to achieving sustainability?, *Chem Rev.* 116 (2016) 7159–7329.
[45] N.T. Thanh Truc, L. Giang Bach, N. Thi Hanh, T.D. Pham, N. Thi Phuong Le Chi, D.T. Tran, M.V. Nguyen, V.N. Nguyen, The superior photocatalytic activity of Nb doped TiO_2/g-C_3N_4 direct Z-scheme system for efficient conversion of CO_2 into valuable fuels, *J. Colloid Interface Sci.* 540 (2019) 1–8.
[46] Y. Liu, F.Y. Su, Y.X. Yu, W.D. Zhang, Nano g-C_3N_4 modified Ti-Fe_2O_3 vertically arrays for efficient photoelectrochemical generation of hydrogen under visible light, *Int. J. Hydrog. Energy* 41 (18) (2016) 7270–7279.
[47] A. Brunetti, F. Scura, G. Barbieri, E. Drioli, Membrane technologies for CO_2 separation, *J. Membr. Sci.* 359 (1–2) (2010) 115–125.
[48] M. Li, X.B. Jiang, G.H. He, Application of membrane separation technology in postcombustion carbon dioxide capture process, *Front. Chem. Sci. Eng.* 8 (2) (2014) 233–239.

[49] Z.Z. Tian, S.F. Wang, Y.T. Wang, X.R. Ma, K.T. Cao, D.D. Peng, X.Y. Wu, H. Wu, Z. Y. Jiang, Enhanced gas separation performance of mixed matrix membranes from graphitic carbon nitride nanosheets and polymers of intrinsic microporosity, *J. Membr. Sci.* 514 (2016) 15–24.

[50] M.J.C. Ordoñez, K.J. BalkusJr, J.P. FerrarisJr, I.H. MusselmanJr, Molecular sieving realized with ZIF-8/Matrimid® mixed-matrix membranes, *J. Membr. Sci.* 361 (1–2) (2010) 28–37.

[51] C. Casado-Coterillo, A. Fernández-Barquín, B. Zornoza, C. Téllez, J. Coronas, Á. Irabien, Synthesis and characterisation of MOF/ionic liquid/chitosan mixed matrix membranes for CO_2/N_2 separation, *RSC Adv.* 5 (124) (2015) 102350–102361.

[52] J.Y. Yu, F.L. Chi, Y.P. Sun, J.J. Guo, X.G. Liu, Assembled porous Fe_3O_4@g-C3N4 hybrid nanocomposites with multiple interface polarization for stable microwave absorption, *Ceram. Int.* 44 (16) (2018) 19207–19216.

[53] R. Peymanfar, J. Karimi, R. Fallahi, Novel, promising, and broadband microwave-absorbing nanocomposite based on the graphite-like carbon nitride/CuS, *J. Appl. Polym. Sci.* 137 (9) (2020) 48430.

[54] Y.J. Ji, H.L. Dong, H.P. Lin, L.L. Zhang, T.J. Hou, Y.Y. Li, Heptazine-based graphitic carbon nitride as an effective hydrogen purification membrane, *RSC Adv.* 6 (57) (2016) 52377–52383.

[55] S.W. de Silva, A. Du, W. Senadeera, Y. Gu, Strained graphitic carbon nitride for hydrogen purification, *J. Membr. Sci.* 528 (2017) 201–205.

[56] Y. Guo, C.M. Tang, X.B. Wang, C. Wang, L. Fu, Density functional calculations of efficient H_2 separation from impurity gases (H_2, N_2, H_2O, CO, Cl_2, and CH_4) *via* bilayer g-C_3N_4 membrane, *Chinese Phys. B* 28 (4) (2019) 048102.

[57] J.M. Hou, Y.Y. Wei, S. Zhou, Y.J. Wang, H.H. Wang, Highly efficient H_2/CO_2 separation via an ultrathin metal-organic framework membrane, *Chem. Eng. Sci.* 182 (2018) 180–188.

[58] M. Soto-Herranz, M. Sánchez-Báscones, A. Hérnandez-Giménez, J.I. Calvo-Díez, J. Martín-Gil, P. Martín-Ramos, Effects of protonation, hydroxylamination, and hydrazination of g-C3N4 on the performance of matrimid®/g-C3N4 membranes, Nanomaterials (Basel) 8 (12) (2018) E1010.

[59] A. Jomekian, B. Bazooyar, J. Esmaeilzadeh, R.M. Behbahani, Highly CO_2 selective chitosan/g-C_3N_4/ZIF-8 membrane on polyethersulfone microporous substrate, *Sep. Purif. Technol.* 236 (2020) 116307.

[60] N.X. Wang, S.L. Ji, G.J. Zhang, J. Li, L. Wang, Self-assembly of graphene oxide and polyelectrolyte complex nanohybrid membranes for nanofiltration and pervaporation, *Chem. Eng. J.* 213 (2012) 318–329.

[61] D.P. Suhas, A.V. Raghu, H.M. Jeong, T.M. Aminabhavi, Graphene-loaded sodium alginate nanocomposite membranes with enhanced isopropanol dehydration performance *via* a pervaporation technique, *RSC Adv.* 3 (38) (2013) 17120.

[62] J.K. Wu, C.C. Ye, W.H. Zhang, N.X. Wang, K.R. Lee, Q.F. An, Construction of well-arranged graphene oxide/polyelectrolyte complex nanoparticles membranes for pervaporation ethylene glycol dehydration, *J. Membr. Sci.* 577 (2019) 104–112.

[63] S.P. Dharupaneedi, R.V. Anjanapura, J.M. Han, T.M. Aminabhavi, Functionalized graphene sheets embedded in chitosan nanocomposite membranes for ethanol and isopropanol dehydration *via* pervaporation, *Ind. Eng. Chem. Res.* 53 (37) (2014) 14474–14484.

[64] R.L.G. Lecaros, K.M. Deseo, W.S. Hung, L.L. Tayo, C.C. Hu, Q.F. An, H.A. Tsai, K.R. Lee, J.Y. Lai, Influence of integrating graphene oxide quantum dots on the fine structure characterization and alcohol dehydration performance of pervaporation composite membrane, *J. Membr. Sci.* 576 (2019) 36–47.

[65] R.A. Kirk, M. Putintseva, A. Volkov, P.M. Budd, The potential of polymers of intrinsic microporosity (PIMs) and PIM/graphene composites for pervaporation membranes, *BMC Chem. Eng.* 1 (1) (2019) 1–19.

[66] R. Castro-Muñoz, J. Buera-González, Ó.D.L. Iglesia, F. Galiano, V. Fíla, M. Malankowska, C. Rubio, A. Figoli, C. Téllez, J. Coronas, Towards the dehydration of ethanol using pervaporation cross-linked poly(vinyl alcohol)/graphene oxide membranes, *J. Membr. Sci.* 582 (2019) 423–434.

[67] H. Jin, K. Mo, F. Wen, Y.S. Li, Preparation and pervaporation performance of CAU-10-H MOF membranes, *J. Membr. Sci.* 577 (2019) 129–136.

[68] X.Y. Zou, M.S. Li, S.Y. Zhou, C. Chen, J. Zhong, A.L. Xue, Y. Zhang, Y.J. Zhao, Diffusion behaviors of ethanol and water through g-C3N4-based membranes: Insights from molecular dynamics simulation, *J. Membr. Sci.* 585 (2019) 81–89.

[69] Q.W. Gao, Y.D. Zhu, Y. Ruan, Y.M. Zhang, W. Zhu, X.H. Lu, L.H. Lu, Effect of adsorbed alcohol layers on the behavior of water molecules confined in a graphene nanoslit: A molecular dynamics study, *Langmuir* 33 (42) (2017) 11467–11474.

[70] J. Campbell, G. Szekely, R.P. Davies, D.C. Braddock, A.G. Livingston, Fabrication of hybrid polymer/metal organic framework membranes: mixed matrix membranes versus in situ growth, *J. Mater. Chem. A* 2 (2014) 9260–9271.

[71] J. Wang, M.S. Li, S.Y. Zhou, A.L. Xue, Y. Zhang, Y.J. Zhao, J. Zhong, Q. Zhang, Graphitic carbon nitride nanosheets embedded in poly(vinyl alcohol) nanocomposite membranes for ethanol dehydration *via* pervaporation, *Sep. Purif. Technol.* 188 (2017) 24–37.

[72] J. Wang, M.S. Li, S.Y. Zhou, A.L. Xue, Y. Zhang, Y.J. Zhao, J. Zhong, Controllable construction of polymer/inorganic interface for poly(vinyl alcohol)/graphitic carbon nitride hybrid pervaporation membranes, *Chem. Eng. Sci.* 181 (2018) 237–250.

[73] C. Shi, C. Lv, L. Wu, X. Hou, Porous chitosan/hydroxyapatite composite membrane for dyes static and dynamic removal from aqueous solution, *J. Hazard. Mater.* 338 (2017) 241–249.

[74] Z.J. Yuan, X.L. Wu, Y.J. Jiang, Y.F. Li, J.J. Huang, L. Hao, J. Zhang, J.T. Wang, Carbon dots-incorporated composite membrane towards enhanced organic solvent nanofiltration performance, *J. Membr. Sci.* 549 (2018) 1–11.

[75] Y. Zhang, S. Zhang, J. Gao, T.S. Chung, Layer-by-layer construction of graphene oxide (GO) framework composite membranes for highly efficient heavy metal removal, *J. Membr. Sci.* 515 (2016) 230–237.

[76] P. Zhang, J.L. Gong, G.M. Zeng, C.H. Deng, H.C. Yang, H.Y. Liu, S.Y. Huan, Cross-linking to prepare composite graphene oxide-framework membranes with high-flux for dyes and heavy metal ions removal, *Chem. Eng. J.* 322 (2017) 657–666.

[77] G. Abdi, A. Alizadeh, S. Zinadini, G. Moradi, Removal of dye and heavy metal ion using a novel synthetic polyethersulfone nanofiltration membrane modified by magnetic graphene oxide/metformin hybrid, *J. Membr. Sci.* 552 (2018) 326–335.

[78] J. Ma, Y. He, G.Y. Zeng, F. Li, Y.B. Li, J.F. Xiao, S.Z. Yang, Bio-inspired method to fabricate poly-dopamine/reduced graphene oxide composite membranes for dyes and heavy metal ion removal, *Polym. Adv. Technol.* 29 (2) (2018) 941–950.

[79] Q.Y. Gan, W.L. Shi, Y.J. Xing, Y. Hou, A polyoxoniobate/g-C_3N_4 nanoporous material with high adsorption capacity of methylene blue from aqueous solution, *Front. Chem.* 6 (2018) 7.

[80] H.C. Lan, F. Wang, M. Lan, X.Q. An, H.J. Liu, J.H. Qu, Hydrogen-bond-mediated self-assembly of carbon-nitride-based photo-Fenton-like membranes for wastewater treatment, *Environ. Sci. Technol.* 53 (12) (2019) 6981–6988.

[81] I. Papailias, N. Todorova, T. Giannakopoulou, N. Ioannidis, N. Boukos, C.P. Athanasekou, D. Dimotikali, C. Trapalis, Chemical vs thermal exfoliation of g-C_3N_4 for NO_x removal under visible light irradiation, *Appl. Catal. B: Environ.* 239 (2018) 16–26.

[82] K. Xiao, P. Giusto, L.P. Wen, L. Jiang, M. Antonietti, Nanofluidic ion transport and energy conversion through ultrathin free-standing polymeric carbon nitride membranes, *Angew. Chem. Int. Ed. Engl.* 57 (32) (2018) 10123–10126.

[83] Y. Wang, L. Li, Y. Wei, J. Xue, H. Chen, L. Ding, J. Caro, H. Wang, Water transport with ultralow friction through partially exfoliated g-C_3N_4 nanosheet membranes with self-supporting pacers, *Angew. Chem. Int. Edit.* 56 (2017) 8974–8980.

[84] Y. Wang, N.N. Wu, Y. Wang, H. Ma, J.X. Zhang, L.L. Xu, M.K. Albolkany, B. Liu, Graphite phase carbon nitride based membrane for selective permeation, *Nat. Commun.* 10 (1) (2019) 2500.

[85] A.A. Aziz, K.C. Wong, P.S. Goh, A.F. Ismail, I.W. Azelee, Tailoring the surface properties of carbon nitride incorporated thin film nanocomposite membrane for forward osmosis desalination, *J. Water Process Eng.* 33 (2020) 101005.

[86] W.Y. Ye, H.W. Liu, F. Lin, J.Y. Lin, S.F. Zhao, S.S. Yang, J.W. Hou, S.G. Zhou, B. van der Bruggen, High-flux nanofiltration membranes tailored by bio-inspired co-deposition of hydrophilic g-C_3N_4 nanosheets for enhanced selectivity towards organics and salts, *Environ. Sci. Nano* 6 (10) (2019) 2958–2967.

[87] Y. Wang, L. Liu, J. Xue, J. Hou, L. Ding, H. Wang, Enhanced water flux through graphitic carbon nitride nanosheets membrane by incorporating polyacrylic acid, *AIChE J.* 64 (2018) 2181–2188.

[88] Y.L. Liu, X.M. Wang, X.Q. Gao, J.F. Zheng, J. Wang, A. Volodin, Y.F. Xie, X. Huang, B. van der Bruggen, J.Y. Zhu, High-performance thin film nanocomposite membranes enabled by nanomaterials with different dimensions for nanofiltration, *J. Membr. Sci.* 596 (2020) 117717.

[89] L. Jiang, X. Yuan, G. Zeng, Z. Wu, J. Liang, X. Chen, L. Leng, H. Wang, H. Wang, Metal-free efficient photocatalyst for stable visible-light photocatalytic degradation of refractory pollutant, *Appl. Catal. B-Environ.* 221 (2018) 715–725.

[90] T. Sata, Studies on ion exchange membranes with permselectivity for specific ions in electrodialysis, *J. Membr. Sci.* 93 (2) (1994) 117–135.

[91] Z. Jiang, W. Wan, H. Li, S. Yuan, H. Zhao, P.K. Wong, A hierarchical Z-Scheme α-Fe_2O_3/g-C_3N_4 hybrid for enhanced photocatalytic CO_2 reduction, *Adv. Mater.* 30 (2018) 1706108.

[92] N. Hou, W. Sun, F. Du, H. Wu, Effect of (super)alkali doping on the electronic and second-order nonlinear optical properties of graphitic C_3N_4, *Optik* 183 (2019) 455–462.

[93] A. Alshahrie, M.O. Ansari, High performance supercapacitor applications and DC electrical conductivity retention on surfactant immobilized macroporous ternary polypyrrole/graphitic-C3N4@Graphene nanocomposite, *Electron. Mater. Lett.* 15 (2) (2019) 238–246.

[94] F.L. Fu, Q. Wang, Removal of heavy metal ions from wastewaters: A review, *J. Environ. Manage.* 92 (3) (2011) 407–418.

[95] Z.T. Wu, L. Gao, J. Wang, F.G. Zhao, L.L. Fan, D. Hua, S. Japip, J.R. Xiao, X.J. Zhang, S.F. Zhou, G.W. Zhan, Preparation of glycine mediated graphene oxide/g-C_3N_4 lamellar membranes for nanofiltration, *J. Membr. Sci.* 601 (2020) 117948.

[96] F. Wang, G. Wang, J.C. Zhang, B.Q. Li, J. Zhang, J. Deng, J.W. Chen, R.L. Wang, Novel sulfonated poly(ether ether ketone)/oxidized g-C3N4 composite membrane for vanadium redox flow battery applications, *J. Electroanal. Chem.* 797 (2017) 107–112.

[97] B. Liu, Y.X. Zhang, Y.H. Jiang, P.H. Qian, H.F. Shi, High performance acid-base composite membranes from sulfonated polysulfone containing graphitic carbon nitride nanosheets for vanadium redox flow battery, *J. Membr. Sci.* 591 (2019) 117332.

[98] L.L. Qu, G. Zhu, J. Ji, T.P. Yadav, Y.J. Chen, G.H. Yang, H. Xu, H.T. Li, Recyclable visible light-driven O-g-C_3N_4/graphene oxide/*N*-carbon nanotube membrane

for efficient removal of organic pollutants, *ACS Appl. Mater. Interfaces* 10 (49) (2018) 42427–42435.
[99] M.M. Pendergast, E.M.V. Hoek, A review of water treatment membrane nanotechnologies, *Energy Environ. Sci.* 4 (6) (2011) 1946.
[100] M.J. Chang, W.N. Cui, J. Liu, K. Wang, X.J. Chai, Fabrication and photocatalytic properties of flexible g-C_3N_4/SiO_2 composite membrane by electrospinning method, *J. Mater. Sci.: Mater. Electron.* 29 (8) (2018) 6771–6778.
[101] T.S. Wong, S.H. Kang, S.K.Y. Tang, E.J. Smythe, B.D. Hatton, A. Grinthal, J. Aizenberg, Bioinspired self-repairing slippery surfaces with pressure-stable omniphobicity, *Nature* 477 (2011) 443–447.
[102] Y.B. Wei, Y.X. Zhu, Y.J. Jiang, Photocatalytic self-cleaning carbon nitride nanotube intercalated reduced graphene oxide membranes for enhanced water purification, *Chem. Eng. J.* 356 (2019) 915–925.
[103] Q.J. Xiang, J.G. Yu, M. Jaroniec, Preparation and enhanced visible-light photocatalytic H2-production activity of graphene/C_3N_4 Composites, *J. Phys. Chem. C* 115 (15) (2011) 7355–7363.
[104] F. Dong, Z. Zhao, T. Xiong, Z. Ni, W. Zhang, Y. Sun, W.K. Ho, *In situ* construction of g-C_3N_4/g-C_3N_4 metal-free heterojunction for enhanced visible-light photocatalysis, *ACS Appl. Mater. Interfaces* 5 (21) (2013) 11392–11401.
[105] Q. Zhang, S. Chen, X.F. Fan, H.G. Zhang, H.T. Yu, X. Quan, A multifunctional graphene-based nanofiltration membrane under photo-assistance for enhanced water treatment based on layer-by-layer sieving, *Appl. Catal. B: Environ.* 224 (2018) 204–213.
[106] H.X. Zhao, S. Chen, X. Quan, H.T. Yu, H.M. Zhao, Integration of microfiltration and visible-light-driven photocatalysis on g-C3N4 nanosheet/reduced graphene oxide membrane for enhanced water treatment, *Appl. Catal. B: Environ.* 194 (2016) 134–140.
[107] N.H. Alias, J. Jaafar, S. Samitsu, T. Matsuura, A.F. Ismail, M.H.D. Othman, M.A. Rahman, N.H. Othman, N. Abdullah, S.H. Paiman, N. Yusof, F. Aziz, Photocatalytic nanofiber-coated alumina hollow fiber membranes for highly efficient oilfield produced water treatment, *Chem. Eng. J.* 360 (2019) 1437–1446.